Molecular Dynamics Study of Lead on Copper (100)

Cathal Dunne (B.Sc.)

School of Physical Sciences

Dublin City University

A thesis submitted to

for the degree of

Master of Science

Research Supervisor

Dr. A.A. Cafolla

September 2001

Declaration

I hereby certify that this material, which I now submit for assessment on the programme of study leading to the award of Master of Science is entirely my own work and has not been taken from the work of others save and to the extent that such work has been cited and acknowledged within the text of my own work.

Signed : Cathal Dunne
Cathal Dunne

ID Number : 97970085

Date : 7/8/01

Contents

Abstract

This project uses the Molecular Dynamics (MD) technique to study the deposition of lead on the (100) face of copper. Integration of the equations of motion is done using the Verlet algorithm. Two potential energy functions are used to model the particle interactions. The first is a two-body Lennard-Jones potential while the second is a three-body Erkoç *potential*.

The deposition of lead on the (100) face of copper results in the formation of three distinct structures as the coverage is varied. In order of increasing coverage they are : c(4×4), c(2×2) and c($5\sqrt{2} \times \sqrt{2}$)R45° reconstructions. The c(4×4) structure is not well understood. It has been ascertained that it's structure is that of a single-layer surface alloy. Chains of copper run parallel and alternately with chains of lead. The two most likely structures are the hollow and bridge alloy models. The current project applied the MD technique to determining which of the two structures was the most likely. It turned out that the bridge alloy model was the most likely using Molecular Dynamics. Also a modulation of the alloy copper chains has been documented. This was also studied and the results point to a modulation with an amplitude of around 0.3Å and a period of 4 copper-copper distances. Neighbouring alloy copper chains exhibited modulations that were 180° out of phase. The structure of the c(2×2) reconstruction is well understood. This structure was included for completeness. The c($5\sqrt{2} \times \sqrt{2}$)R45° reconstruction has also been the subject of much study in recent years. Starting with an initial hexagonal-type structure the MD simulation evolved the accepted structure for the c($5\sqrt{2} \times \sqrt{2}$)R45° reconstruction.

Acknowledgements

I would like to thank my parents and family for their help and support throughout my time in university. I am forever grateful to them. I would also like to thank Tony Cafolla, my supervisor, for his constant and insightful suggestions, without which progress would have been very difficult. I would also like to thank my fellow postgrads : Jason, Ian, Clodagh, Eilish, Mark to name a few, for their help and humour. I would also like to thank Greg Hughes for his useful discussions and good humour. Finally I would like to thank Enterprise Ireland who provided part payment of my course fees.

Chapter 1 Introduction

The origins of molecular dynamics (MD) date back to the atomism of antiquity. The constituents, although from a more recent time, are not exactly new. The theoretical foundations amount to little more than Newton's Laws of motion. The importance of the solution to the many-body problem was recognised by Laplace : *"Given for one instant an intelligence which could comprehend all the forces by which nature is animated and the respective situation of the beings who compose it – an intelligence sufficiently vast to submit these data to analysis – it would embrace in the same formula the movements of the greatest bodies of the universe and those of the lightest atom : for it, nothing would be uncertain and the future, as the past would be present to it's eyes."* The concept of the computer dates back to the time of Babbage. Thus MD is a methodology whose appearance was a foregone conclusion.

The N-body problem originated in the dynamics of the solar system, and the general problem turns out to be insoluble for three or more bodies. A great deal of the behaviour of matter in its various states can be understood in classical (meaning non-quantum) terms, and so it is that the classical N-body problem is also central to understanding matter at the microscopic level. MD addresses the task of the numerical solution of this problem. Theory in the form of statistical mechanics, has met with a considerable degree of success for systems in thermal equilibrium. Systems that are in a non-equilibrium state are however virtually unapproachable using ststistical mechanics. Generally it is only by means of computer simulation – principally molecular dynamics – that progress is possible.

The aim of this project is to study the structure of the Pb/Cu(100) interface for lead coverages up to 1ML, using the MD technique. When lead is deposited on the (100) face of copper, three reconstructions form as the coverage is increased from 0 monolayers (ML) to 0.6ML. One monolayer corresponds to one lead atom per

(1×1) substrate unit cell. At a coverage of 0.375ML a c(4×4) reconstruction forms, a c(2×2) reconstruction forms at a coverage of 0.5ML and a c($5\sqrt{2}\times\sqrt{2}$)R45° structure forms at a coverage of 0.6ML. The structure of the c(2×2) and c($5\sqrt{2}\times\sqrt{2}$)R45° reconstructions are well established. The c(4×4) reconstruction however remains unclear and has been the focus of much lead on copper (100) work, both experimental and theory, over recent years. All three reconstructions are considered in the current project.

It was originally proposed that the c(4×4) reconstruction involved chains of lead atoms with adjacent chains being 2 nearest-neighbour copper-copper distances out of phase. This model was named the chain model [**2**]. Later an STM study[**3**] asserted that the c(4×4) reconstruction was a surface alloy with the unit cell corner atoms sitting in bridge sites. This was concluded from the fact that every third lead atom along a lead chain was brighter in the STM image. The explanation given was that the brighter atoms must be sitting on bridge sites. This model was named the bridge alloy model. Recently a I/V LEED calculation [**4**] was done to determine which of the hollow chain model, bridge chain model, hollow alloy model or bridge alloy models was the most likely structure for the c(4×4) reconstruction. It was concluded from the results that the hollow alloy model was the most likely structure for the c(4×4) reconstruction. Also from this study it was revealed that there was a modulation of the alloy copper chains that lie alternately between the alloy lead chains. A further STM study [**5**] asserted that the c(4×4) reconstruction is a surface alloy, however the hollow or bridge alloy models are not favoured. A Monte Carlo (MC) simulation [**6**]of the c(4×4) system concludes that the alloy copper modulation has a period of approximately 8 copper-copper distances along a chain. The potential energy function used in the previous MC study is one of two potentials investigated in the current project, the second being a three-body Erkoς potential. The MC simulation concluded that the hollow and bridge alloy models were both equally likely. The aim of the current study is to ascertain which of the hollow or bridge alloy models is the most likely using the MD technique. Also the

exact details of the alloy copper modulation are studied.

The c(2×2) reconstruction occurs at a coverage of 0.5ML. The exact structure of this reconstruction is well known. It is considered in the current study for completeness. Also the results may reveal any modulations of the lead layer or the underlying substrate layer.

The exact structure of the c($5\sqrt{2} \times \sqrt{2}$)R45° reconstruction is also well established. Initially a hexagonal-type structure was proposed. Further studies revealed that anti-phase domain boundary insertion was the mechanism from which the lower coverage c(2×2) reconstruction proceeded towards the c($5\sqrt{2} \times \sqrt{2}$)R45° reconstruction with increasing coverage. The STM results show alternate strips of 3 rows of c(2×2) structure separated by regular occuring anti-phase domain boundaries. This has become the accepted structure for the c($5\sqrt{2} \times \sqrt{2}$)R45° reconstruction and was verified by further STM studies. The aim in the current MD work for the c($5\sqrt{2} \times \sqrt{2}$)R45° reconstruction is to try to evolve the accepted reconstruction from an initial configuration that corresponds with the hexagonal structure mentioned above.

By studying the c(4×4) structure of Pb on Cu(100) it may be possible to infer the structures of other systems such as Tl on Cu(100) which may well turn out to be a single layer surface alloy which is unusual for metal overlayers on metallic substrates. Single layer surface alloying has also been shown for the Ni on Cu(100) system. Thus it is interesting from an academic point of view to study the Pb on Cu(100) system.

Chapter 2 Simulation Method

In this chapter the essential program operations are explained after which the program flow, ie. the sequence of operations, is given.

Section 2.1 explains the reduction of units which is important for any molecular dynamics simulation.

The initial system conditions are given in Section 2.5. This involves a detailed description of how initial coordinates, velocities and accelerations are calculated. Some reference is made to the Neighbour Listing method which is covered in Section 2.3.

The rules governing the behaviour of particles at the boundaries of the simulation region are explained in Section 2.2. This includes a description of Periodic Boundary Conditions.

Section 2.3 describes the Neighbour Listing method. The criteria for rebuilding the neighbour lists are given here also as well as the main force loops.

The Verlet algorithm, which integrates Newtons equations of motion, is explained in Section 2.4.

The final Section gives a description of the program flow. The program operations explained in previous sections are combined using a time loop which steps the coordinates, velocities and accelerations forward in time using a time counter.

2.1 Reduction of Units

The current implementation of molecular dynamics (*MD*) involves following the positions, velocities and accelerations of copper and lead atoms in a crystal. As time evolves the atoms move around in thermal motion. The nearest-neighbour separations are on the order of a few angstroms (10^{-10}m). The computer must be able to accomodate such small numerical values in memory. It is important to ensure that none of the program variables aquire values that fall outside the range of

numbers that the computer hardware is capable of handling. To do this we express length as a multiple of one angstrom. A length of 0.01Å would hence be stored in memory as the value 0.01 as opposed to 0.000000000001. This unit of length is called a reduced length unit for our system. When calculating velocities for example this new reduced unit of length must be taken into account. The following set of reduced units were adopted.

- *Length* - multiples of one angstrom, 1Å

$$l_r = l_{SI}/1\mathring{A} \tag{1}$$

l_r = reduced length (Å)
l_{SI} = SI length (metres)

- *Energy* - multiples of one electron volt, $1eV$

$$E_r = E_{SI}/1eV \tag{2}$$

E_r = reduced energy (eV)
E_{SI} = SI energy (Joules)

- *Mass* - multiples of one atomic mass unit, $1amu$

$$m_r = m_{SI}/1amu \tag{3}$$

m_r = reduced mass (amu)
m_{SI} = SI mass (Kilogram)

Using this unit reduction scheme all other *MD* quantities can be expressed in reduced units which are more favourable for the computer hardware. Note that the unit of temperature is left as degrees Kelvin which is also the standard international (SI) unit. Temperature multiplied by Boltzmanns constant k_b, results in a value corresponding to thermal energy. The SI unit of k_b is joules/Kelvin. Our reduced unit for energy however is the Electron Volt (eV) thus the reduced value of k_b is given by

- Boltzmanns constant(k_b) - multiples of one electron volt per Kelvin, $1eV/Kelvin$

$$^{(r)}k_b = {}^{(SI)}k_b/1eV \tag{4}$$

$^{(r)}k_b$ = reduced Boltzmanns constant (eV/K)
$^{(SI)}k_b$ = SI Boltzmanns constant (joules/kelvin)

Hence the new unit for Boltzmanns constant is eV/K. By multiplying $^{(r)}k_b$ by a temperature in Kelvin we are left with a thermal energy with units of electron volts.

The reduced unit of time is defined by the *lead-lead* interaction **[6]** and the lead mass, m. The depth of the Lennard-Jones *lead-lead* potential is labeled ϵ while the nearest-neighbour distance is designated σ. The reduced unit of time, τ, is calculated using :

$$\tau = \sigma \times \sqrt{\frac{m}{\epsilon}}$$

By inserting the parameter values as found in Chapter 3, section 3.5.1, the unit of time for the system turns out to be 1.3×10^{-13}s. The time step chosen is 1/100 of this value giving a *MD* time step on the order of femto seconds which is typical for *Molecular Dynamics* simulations.

2.2 Boundary Conditions

The simulation region is the range of x, y and z values through which the particles in the system can move. The (100) surface of the copper substrate is in the x-y plane with the z direction being normal to the surface. Atoms in the bottom layer are held fixed. There are no restrictions on the possible z values of the moveable atoms. This is called a *Free Boundary Condition.*

2.2.1 Periodic Boundary Conditions

The boundaries in the x and y directions follow *Periodic Boundary Conditions* (PBC). The current system attempts to mimic the real system, however a real system contains a very large number of atoms compared to the number that can be

represented on a computer. The real system has infinite extent in relative terms. In order to mimic the real infinite system in molecular dynamics the PBC technique is used.

When a layer of lead is deposited on a copper substrate the first three to four substrate layers are affected. This fact means that the current approach, which uses four copper substrate layers, is sufficient to mimic the real system. The number of atoms in the planes parallel to the surface in the real system however is relatively very large (10^7 atom/cm). Hence the corresponding *MD* planes need to be bounded in a way that mimics the much larger size of the real system.

The implementation of PBCs is shown schematically in Fig. 2.1.

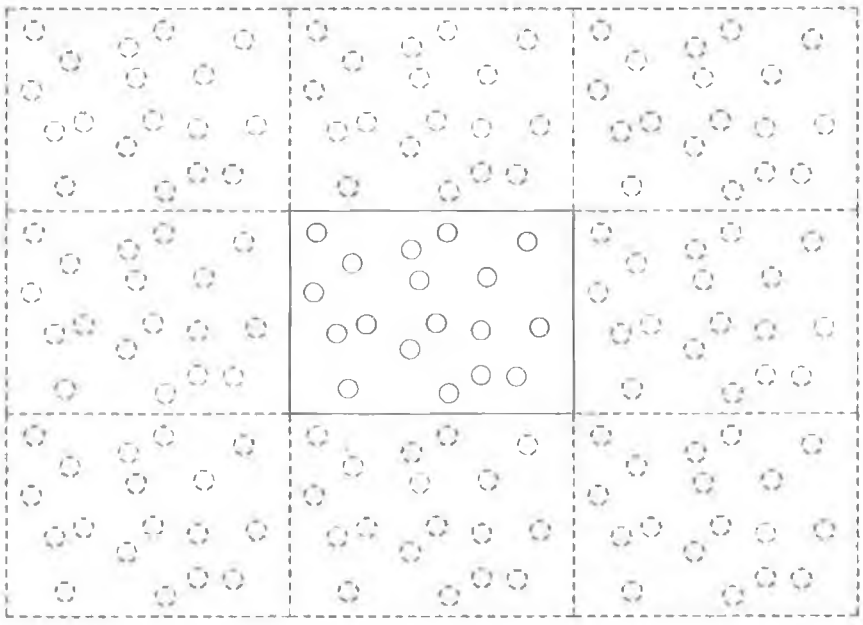

Figure 2.1: Periodic Boundaries

The introduction of PBCs is equivalent to considering an infinite space-filling array of identical copies of the simulation region. There are two consequences of this periodicity. The first is that an atom that leaves the simulation region through a particular bounding face reenters through the opposite face. The second is that atoms lying within a distance $\mathbf{r}_c$ (the cut-off radius for neighbour listing) of a boundary interact with atoms in an adjacent copy of the system, or, equivalently with atoms

near the opposite boundary.

The introduction of periodic boundaries has consequences for both the integration of the equations of motion and the interaction computation of the particle-particle interactions. After each time step the x, y and z values of each particle are updated according to their velocity, acceleration and previous position. If an atom is found to have moved outside the region (x and y directions only) its coordinates must be adjusted so that it reenters through the opposite boundary. Say for example that the x coordinate of a particle is defined to lie between $-L_x/2$ and $L_x/2$, where L_x is the region size in the x direction, then to adhere to PBCs the following tests are carried out.

if $x_i \geq L_x/2$
then $x_i = x_i - L_x$

The particle has reentered on the negative side.

if $x_i \leq L_x/2$
then $x_i = x_i + L_x$

The particle reenters on the positive side. The y direction is treated in an identical manner.

The effect of PBCs on the interaction calculations appears in finding the component separations Δx_{ij} and Δy_{ij} between pairs of atoms. In the above example this is equivalent to asking whether $|\Delta x_{ij}| \geq L_x/2$. If this is true the component separation of particles i and j in the x direction is altered according to :

if $\Delta x_{ij} \geq L_x/2$
then $\Delta x_{ij} = \Delta x_{ij} - L_x$

and

if $\Delta x_{ij} \leq -L_x/2$
then $\Delta x_{ij} = \Delta x_{ij} + L_x$

These are the set of rules used to apply *Periodic Boundary Conditions*. On examination it is clear that the maximum interaction range is limited to $L_x/2$ in the example. This is not an important constraint since the Neighbour List cut-off radius is normally much smaller. In the current work r_c is 25% of L_x and L_y.

2.3 Neighbour Listing Method

The forces on any atom in the simulation are due to every other atom in the system. If, in calculating the force on an atom, every other particle is considered then this scheme is called *All Pairs*. The name is self-evident from the fact that all pairs of atoms are considered when calculating the force on a particular particle. This scheme of course only refers to *atom-atom* interactions. The *Erkoς* potential, described in Chapter 3, includes *atom-atom-atom* contributions also. In what follows *All Pairs* would be relabeled *All Triplets*. Any reference to *All Pairs* will be analagous to *All Triplets*. From the curves of the potentials given in Chapter 3, figures 3.17 and 3.18, it is clear that the pair potential energy approaches a value close to zero beyond a certain pair separation. The slope of the curve in this region is also close to zero, the slope corresponding to the pair interaction force. This means that neighbours beyond this separation will exert substantially less force on an atom compared with neighbours that are closer. For this reason it should be clear that the *All Pairs* method is potentially very inefficient for regions that are relatively large. The *All Pairs* method will include neighbours for which the interaction force is close to zero. These neighbours can be omitted from the force calculation without any loss of accuracy. Excluding these 'long-distance' neighbours in the force calculation is the motivation for using the *Neighbour Listing* method. As mentioned earlier the force calculation in *MD* is normally the most expensive. A schematic diagram of the *All Pairs* and *Neighbour Listing* methods are given in Figure 2.2 below. The Neighbour Listing method involves creating an integer list of the indices of all neighbours within a given cut-off radius, $\mathbf{r}_c$, of a particle. This is repeated for every moveable particle in the region so that on completion every moveable atom in the simulation region has associated with it a list of the indices of all its neighbours that are within a

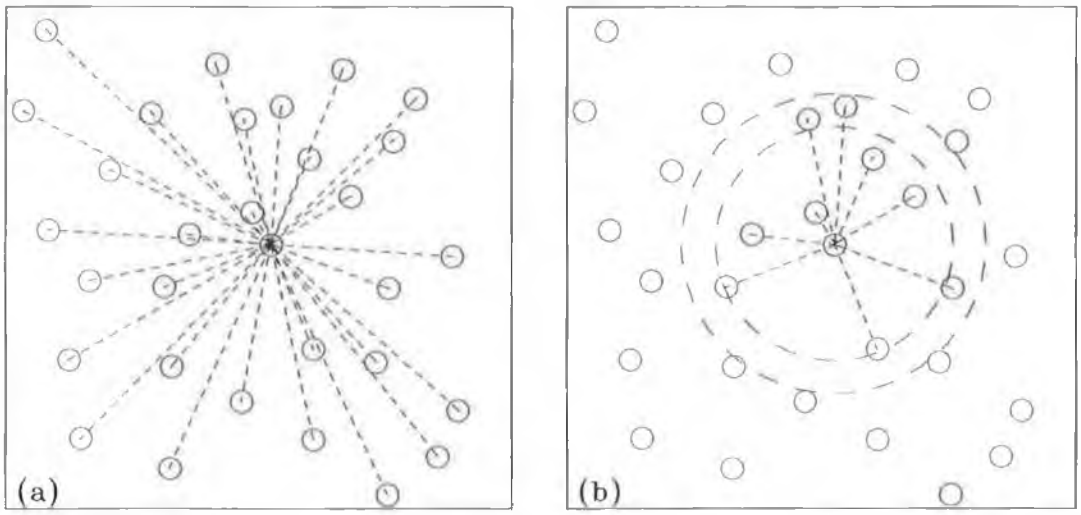

Figure 2.2: All pairs (a) and Neighbour Listing (b)

distance $\mathbf{r}_c$. An atoms index is an integer value, unique to the atom, that is used to refer to that particular particle. If eight hundred particles were involved, their indices would range from 0 - 799. A two-dimensional array would be sufficient to hold the Neighbour List, however the *C* language *structure* data type is used for clarity. An array of structures is then used, one structure for each moveable atom. Each structure contains an integer array which holds the neighbour indices and a single integer variable which indicates the actual number of neighbours in the corresponding array. Fixed particles do not require a neighbour list. These particles never move, therefore it would be pointless to construct lists of neighbours for each of them. As mentioned earlier, a particle's neighbour list contains a list of those nearest neighbours that are within a distance $\mathbf{r}_c$ of that particle. Only a particle's neighbour list entries are used in determining the net force on a particle.

The disadvantages of adopting Neighbour Listing are that storage needs to be provided to hold the list entries in memory and the neighbour lists of the moveable particles will need to be rebuilt at certain times during the *MD* program. This is explained below.

If no extra neighbours come within a distance $\mathbf{r}_c$ of a particular particle over a range of time steps then the same set of neighbours can be used for the force

calculations over that range of time steps. This does not mean that the force on that particle will remain unchanged over this range since its neighbours positions will have changed at every time step hence changing the particle's local environment. If a new particle comes within a distance $\mathbf{r}_c$ of a particle, the neighbour list for that particle will have to be revised to allow for the 'new' neighbour, ie. its neighbour list will have to be rebuilt. To avoid monitoring every paticle's neighbours in this way, which would be computationally expensive, the checking is done globally. The motion of every particle can be monitored by finding the maximum velocity over all particles at each time step. The maximum distance that any particle in the crystal can move at that time step is then given by the product of the maximum velocity at that time step and the value of the time step. If the maximum distance at each time step is summed over successive time steps then we have an effective measure of a particles maximum distance traveled over a range of time steps. If this summed maximum displacement exceeds a preset distance, then the moveable particle neighbour lists are rebuilt. This is the criterion used to determine when the neighbour lists should be rebuilt. The preset distance is labeled Δr_c. Typically Δr_c is about $20 - 40\%$ of the $\mathbf{r}_c$ value. The optimum value of Δr_c however will depend both on the system temperature and the value of the time step.

The effect of introducing Δr_c into the construction of the neighbour lists is that now neighbours within a distance of $r_c + \Delta r_c$ are included. The actual value of r_c should still be chosen as described earlier in this section. Fig. 2.3 below shows a schematic diagram in 2-D to illustrate the included neighbours. Since Δr_c is the upper bound for the summed maximum displacement, no atoms beyond a distance of $r_c + \Delta r_c$ can move to a distance of r_c before the neighbour lists are rebuilt. This ensures that a particles list of neighbours can be used legitimately over a range of time steps when calculating the net force on that particle. It also greatly improves program efficiency since the neighbour lists now only require reconstruction every x number of time steps. The frequency of reconstruction depends on the summed maximum displacement, hence this frequency will be higher for higher temperatures where particles have higher velocities. To counteract this, one may need to increase

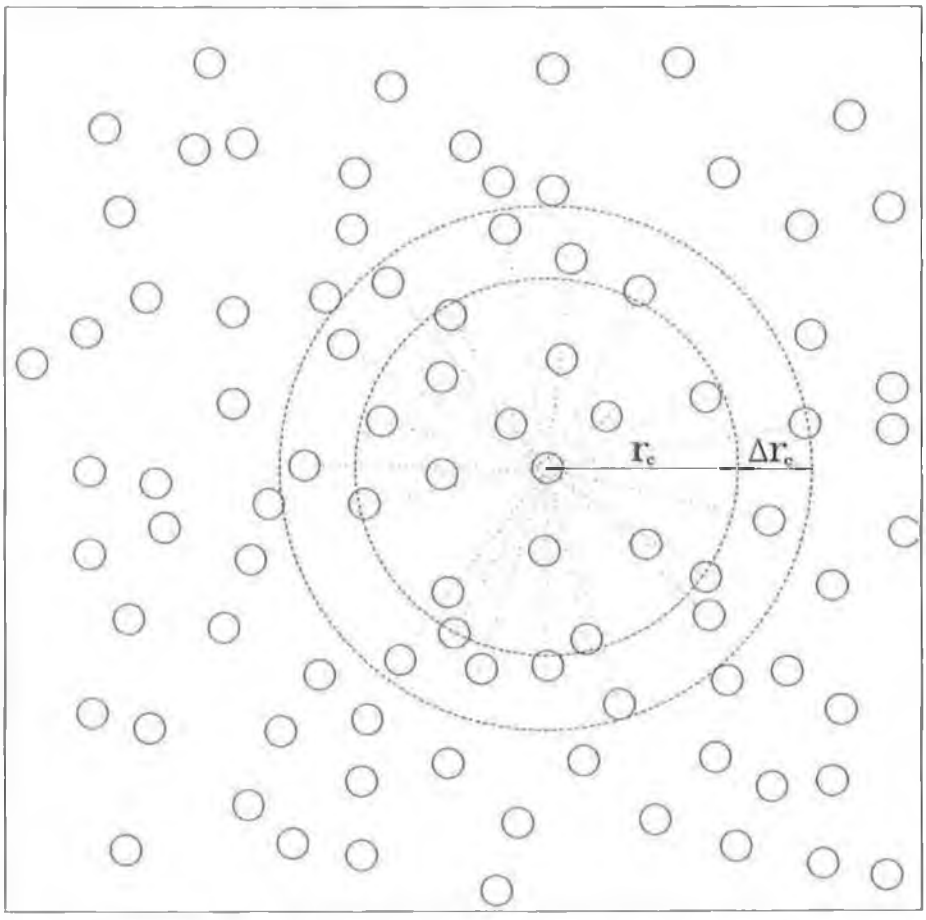

Figure 2.3: Included neighbours in Neighbour Listing

the value of Δr_c for higher temperatures. This lowers the rate of neighbour list reconstruction. The optimum rebuilding rate is specific to the particular system.

The criterion for rebuilding every moveable particles neighbour list is formally given below. The index i refers to every moveable particle.

if

$$\sum_{steps} MAX(v_i) \times \Delta t \geq \Delta r_c$$

then

```
Rebuild Neighbour lists
```

The quantity Δt, is the time step value. This test is evaluated at each time step in a function called `NebrTest`. The maximum displacement is the quantity being summed over successive time steps, ie. maximum velocity times Δt.

2.4 Integration Method

Integration of the equations of motion is done using the Verlet algorithm **[10]**. This is simply a method of implementing Newton's Laws of Motion. The integration formulae applied to each component (x component shown only) of an atoms coordinates and velocities are :

$$x_{n+1} = x_n + {}^{(x)}v_n \times \Delta t + \frac{1}{2}{}^{(x)}a_n \times \Delta t^2 \tag{5}$$

$${}^{(x)}v_{n+1} = {}^{(x)}v_n + \frac{({}^{(x)}a_{n+1} + {}^{(x)}a_n)}{2} \times \Delta t \tag{6}$$

The subscript n represents the time step so that 'n' and '$n+1$' refer to consecutive time steps. Both formulae are given for a particles x component. The equations are identical for the y and z components. The velocity and acceleration of the particle are labeled v and a. The acceleration a_n due to each pair interaction is calculated by inserting the relevant values into one of the two force expressions discussed in Chapter 3, sections 3.5.1 and 3.5.2, ie. the expressions derived from the Lennard-Jones potential or the Erkoς potentials.

2.5 Initial Conditions

In this section atom and interaction types are explained. A detailed description is given on the initial coordinates, velocities and accelerations of each lattice particle. A separate program is developed to calculate new particle 'z' component values resulting in a reduction of strain-heating during a typical *MD* run. The exact method of allocating correct component velocities made to correspond to a particular initial temperature is shown. The initial component acceleration values are detailed with respect to the Neighbour Listing method, which is explained in more detail in section 2.3.

Atom and Interaction types

If a crystal lattice is to be simulated then the actual crystal particles must be created. Creation of a particle simply involves allocating storage in the computer memory which will hold the relevant particle variables ie. position, velocity and acceleration. Another essential particle attribute is a particular atoms *type*. In the current project only two atom types are considered, copper and lead. It is very important to distinguish between the two since the atoms type determines how it interacts with its neighbours. Take for example a copper atom in an ideal *Face Centred Cubic* (FCC) lattice of other copper atoms. Assuming that the lattice is unstrained and in temperature equilibrium the atom will oscillate in a small region, which is approximately spherical, about its corresponding FCC lattice site. Its neighbours will do likewise. If however this copper atom is replaced by a lead atom which is 'bigger' (larger nearest-neighbour distance) the surrounding copper neighbours will be repelled. The positions of the neighbours will reorganise and shift to new positions which correspond to a lower overall potential energy. Thus as can be seen from the example an atoms *type*, be it copper or lead, is a vital piece of information when considering the force between a particle and its neighbours. Since the system at hand has two atom types there are three possible *atom-atom* interactions. These are copper-copper, copper-lead and lead-lead. Note that there are 2^3 *three-body* possibilities however with regard to the *Erkoς* potential the *three-body* part is expressed as a sum of weighted *two-body* terms. This is why the discussion is limited to *two-body* potentials.

A full set of interaction parameters are required for each of the possible particle interactions. These are read into the program as part of initialisation. A *structure* type variable in the *C* programming language is used to hold each set while an array of these structures allows all three sets to be stored and referenced easily. The copper-copper, copper-lead and lead-lead parameters are stored in this order respectively. Since arrays in *C* are indexed starting with element zero there is

an obvious choice of values to designate the three possible interaction types. The copper-copper interaction is assigned an integer value of zero, copper-lead a value of one and lead-lead a value of two. These are the three interaction types which allow access to the correct set of interaction parameters. The interaction type (0,1,2) is used as the index for the Parameter array.

The next question is how to compute an interaction type? If the particle type *copper* (CU) is assigned a value of 0 and *lead* (PB) a value of 2 then there is an easy way of calculating interaction types from the constituent particle types. This is done by averaging the atom-types of the two atoms involved in the interaction. The two possible particle types are assigned as follows:

$$\texttt{CU} = 0$$

$$\texttt{PB} = 2$$

The table below shows how interaction types are arrived at using the constituent particle types.

Interaction	average	Interaction Type
CU-CU	$\frac{0+0}{2}$	0
CU-PB	$\frac{0+2}{2}$	1
PB-PB	$\frac{2+2}{2}$	2

By using the resulting interaction type as an index for the parameter array the relevant set of parameters are accessed. In an involved force calculation as occurs with the *Erkoς* potential this is a useful reference system.

Other particle variables, although not essential, are *fix_free* and *layer*. These are integer values that define a particles ability to move freely and the layer to which it belongs respectively. A particle with a *fix_free* value of zero is fixed whereas a particle with a *fix_free* value of one is free to move. A particle in the lowermost (z=0) layer is assigned a *layer* value of zero with 'higher' layers given increasing integer values. A particles *fix_free* and *layer* values help with analysing the output of the program as well as debugging.

2.5.1 Initialising particle variables

The important variables in a molecular dynamics (*MD*) program are the component positions, velocities and accelerations. During a typical *MD* run these are the values that 'flow' and change as time is advanced. These variables change with every time step according to Newton's Laws of motion hence giving rise to the term *Molecular Dynamics*. This enables an experimenter to simulate the time evolution of a physical system making it a very useful method for modeling the dynamic and static properties of a particular system. The static properties usually involve the extraction of a system configuration at zero Kelvin. To reduce the systems temperature to 0K the kinetic energy of each particle must be continously reduced. This is done by scaling down the component velocities of each particle at preset intervals of time. This is analagous to putting the system in contact with a heat sink. In the current project this is exactly the case with enough extraction of kinetic energy to ensure reasonable spatial resolution between individual layers and splittings of layers ('sublayers'). A layer can split into several separate layers called sublayers. These sublayers are more easily discernable if there is minimal random atom displacement due to an atoms temperature. As a particles kinetic energy is continuosly reduced it occupies a sphere of oscillation of decreasing radius. The main motivation in doing this is to pinpoint the exact equilibrium positions of the addlayer lead atoms. In practice a temperature of around 10-20K will suffice for the desired resolution in position. This range however is very dependent on the particular system.

Note that it is very important to initialise the lattice at a temperature very much greater than the final 10-20K range mentioned. The reason for this will be explained below.

2.5.2 Initial positions

The current system involves a *Face Centred Cubic* (100) copper lattice substrate with various lead overlayer structures being laid on 'top'. The 'top' is that surface

which has the maximum z value. The z direction is normal to the copper surface with positive z going in the direction from surface to vacuum.

The simulation region is the range of x, y and z values through which the particles in the system can move. The lowermost (smallest z value, $z = 0$) particles of the copper substrate are not permitted to move and this as a result negates the need to calculate the net forces on these atoms as the simulation advances in time. This improves the program's efficiency since the force calculation in *MD* is usually the most expensive. These atoms will however be included when calculating the forces on atoms that are above the bottom layer and free to move. This fixed layer serves to anchor the lattice creating a rigid base. Any relaxation of near-surface layers will occur relative to this fixed layer which mimics the real case where the infinite internal extent of *bulk* copper is practically unaffected by the presence of the surface. The fixed layer forms the first of 4 copper substrate layers . The upper 3 layers are free to move (non-fixed). Once the substrate layers have been created the adlayer of lead or lead/copper alloy is deposited on the uppermost substrate layer. The exact x and y coordinates of the adlayer are read in from a pre-prepared file. The z values of each layer are read in from a separate file due to reasons described in the following Section. The region size in the x-y plane is 10×10 copper FCC unit cells. Each substrate layer consists of 200 copper atoms. As mentioned above there are 4 copper substrate layers. The number of atoms in an adlayer of lead is less than 200 since there are less lead atoms per unit area compared with copper. The reconstruction being considered is determined by which adlayer input file is used to assign the adlayer x and y values. The number of adlayer particles also needs to be specified in the program so that sufficient storage space is allocated to hold the adlayer variables.

The substrate copper layers are given layer by layer x and y values that correspond to a *Face Centred Cubic* lattice. The cell edge length, a, is calculated from the nearest-neighbour distance of the particular potential energy function. An FCC cell face is shown below. The diagonal length is twice the nearest-neighbour distance. This results in a cell edge length of $\sqrt{2} \times r_{nn}$, where r_{nn} is the nearest-neighbour

separation.

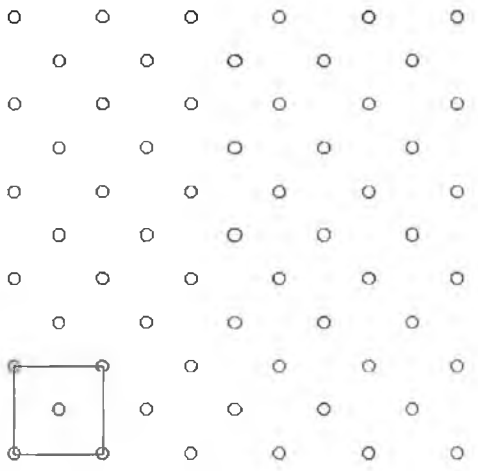

Figure 2.4: FCC (100) face

A Face Centred Cubic lattice can be reproduced by associating each point of a Simple Cubic lattice with three other *basis* atoms which sit at the centre of the three nearest faces of the cubic unit cell. The FCC unit cell has the same dimensions as the underlying cubic unit cell however the FCC unit cell is more dense containing a total of 4 atoms while the corresponding cubic structure has one atom per unit cell. The number density ρ_N is thus given by :

$$\rho_N = 4/a^3$$

This is for bulk copper where the underlying cubic unit cell is an exact cube. Near to the surface where relaxation effects occur, the FCC cell differs slightly from the perfect FCC structure. The cell edge length in the z direction is slightly smaller than the bulk value. This is due to the surface layers relaxing in a direction normal to the surface. This is the reason that bulk FCC 'z' values cannot be applied to the current system.

If the surface consists of a pure copper layer there are no surface effects in the x and y directions. This fact changes however when the pure surface copper layer is replaced by a species other than copper, such as lead. This occurs because the lead layer does not sit 'comfortably' on the copper substrate. Lead has a much larger nearest-neighbour (32% greater) separation which results in a shifting of most

near-surface atoms and surface atoms to more energetically favourable positions, specifically to positions that correspond to a lower total potential energy. This is one of the main topics of interest in this project.

The x and y values of the substrate are assigned values that correspond with a perfect FCC lattice. This is done by creating a simple cubic lattice with edge length **a**. Note that to begin with the perfect FCC lattice is created and only after are the z positions of each layer changed to accomodate the near-surface strain effects. The number of FCC unit cells in each of the component directions is specified by the three numbers N_x, N_y and N_z. Thus the region size is determined by the required number of FCC unit cells. This will also determine the number of substrate particles to be included. The unit cell edge length, which is the same in each direction to begin with, is given by A_x, A_y and A_z. Since the z positions will later be changed, as mentioned above, the z cell edge length turns out to be somewhat unnecessary. Using the number of cells in each component direction and the cell edge length in each direction a cubic lattice can easily be produced. The coordinates of the cubic lattice points are given below.

Cubic coordinates :

$$(n_x \times A_x \, , n_y \times A_y \, , n_z \times A_z) \tag{7}$$

for

$$n_x \in \{\, 0, \ldots, N_x \,\}$$
$$n_y \in \{\, 0, \ldots, N_y \,\}$$
$$n_z \in \{\, 0, \ldots, N_z \,\}$$

To convert this Cubic lattice into a *Face Centred Cubic* lattice, three basis coordinates, corresponding to basis particles, must be associated with each pure cubic coordinate given in equation (7). The basis coordinates associated with the cubic coordinate given in (7) are as follows.

Basis coordinates :

$$(n_x \times A_x + A_x/2\ ,\ n_y \times A_y + A_y/2\ ,\ n_z \times A_z \qquad) \tag{8}$$

$$(n_x \times A_x + A_x/2\ ,\ n_y \times A_y \qquad ,\ n_z \times A_z + A_z/2) \tag{9}$$

$$(n_x \times A_x \qquad ,\ n_y \times A_y + A_y/2\ ,\ n_z \times A_z + A_z/2) \tag{10}$$

Using this scheme a perfect FCC lattice is formed. The z coordinates however need to be altered due to surface effects as explained below. The coordinates given for the above FCC lattice correspond to *bulk* copper.

2.5.3 Relaxation strain effects

Initially the z positions of the individual layers are assigned values that correspond to bulk copper positions as shown above in equations (8-10). It is assumed that the layers relax during the running of the program to positions that take surface effects into account, ie. relaxation of surface layers due to the proximity of a free surface. This indeed happened however the initial bulk z values turned out to be relatively far from the equilibrium minimum-energy values. With such starting coordinates the lattice is effectively strained in the z direction. During the course of the program as the layers relax and approach their 'preferred' positions there is a translation of the initial excess potential energy (strain) to kinetic energy. This results in a large temperature rise of the system. The temperature increased so drastically in fact that the surface adlayer coordinates were completely disordered. This corresponds to the melting of the adlayer. The ideal starting temperature should be close to but less than the melting temperature of the adlayer. To avoid this initial *strain-heating*, a separate program (**BEST_Zs**) was developed to find initial z layer values that would correspond to a lower initial strain in the z direction.

The strain in the lattice corresponds to an excess potential energy in the system. To reduce this strain the layers are moved to new z values which give a lower global potential energy (GPE). The x and y values remain unchanged, the reason for which was explained in the section on periodic boundary conditions, section 2.2. This procedure of finding a configuration of lower global potential energy is

identical to the *Monte Carlo* (MC) method however the precision required for the current purposes are not as accurate as those found in a typical MC method. A crude method for arriving at a lower potential energy is adopted. Each moveable layer is moved repeatedly until a lower GPE occurs. The corresponding z value is recorded. On exiting, this program will have a new z value for each moveable layer in the system. Using these new z values there will be less initial strain-heating of the crystal in the main *MD* program. Once the initial heating is limited to a value below the melting temperature of the adlayer, typically around 500K, then the new layer z positions were accepted as the initial z values. Separate runs of this BEST_Zs program were run for each of the three lead adlayer reconstructions studied, as well as for both the Lennard-Jones and Erkoς potentials.

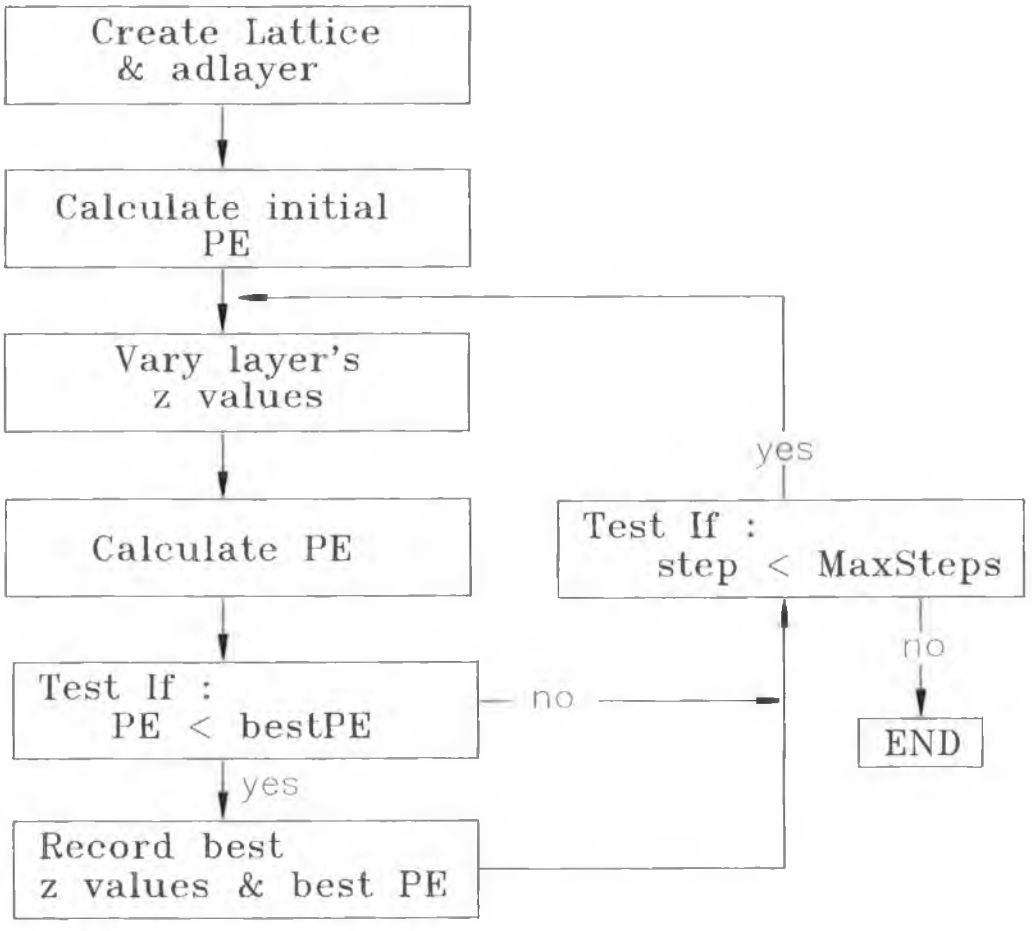

Figure 2.5: Flow diagram of BEST_Zs program

program is given in Fig. 2.5 below. Care was taken not to reduce the strain in the z direction too severely. The reason is that the final state of a system in a *MD* simulation can depend strongly on the initial state. Now, referring back to the BEST_Zs program, the GPE is reduced by varying the layer z positions. If the GPE is reduced too much the resulting system may well have a configuration sitting in a local minimum GPE state. Figure 2.6 below shows this schematically. In order for the system to achieve the GPE minimum configuration it needs to 'jump' the adjacent energy barrier. If there is sufficient sampling of the configuration space the GPE minimum will be achieved. This translates into whether the particles of the lattice have enough kinetic energy to sample various locations. This is the motivation in the *Monte Carlo* method for starting at a relatively high temperature. A simulated annealing process then allows *MC* to approach a GPE minimum configuration.

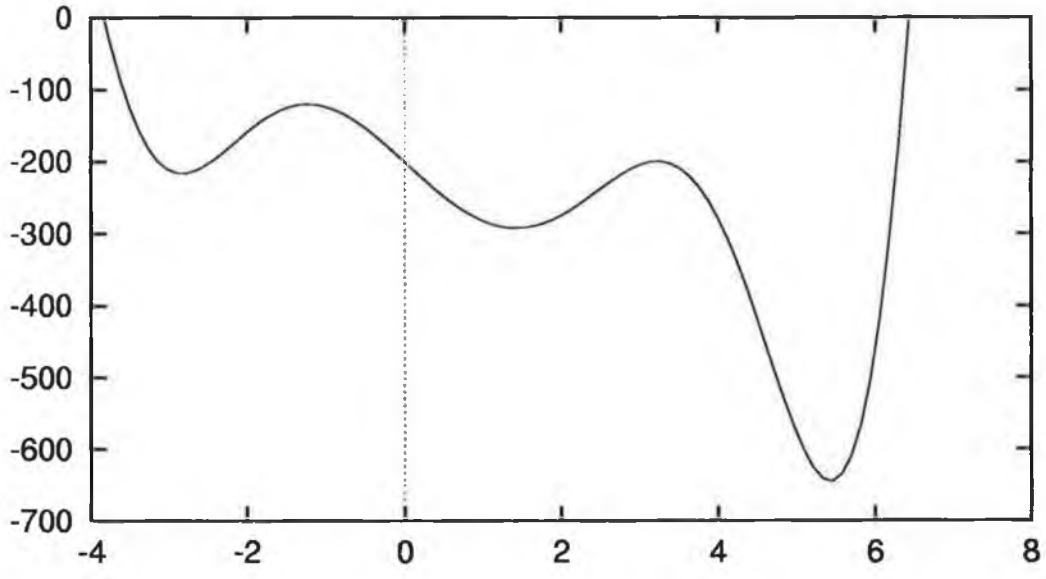

Figure 2.6: GPE vs configuration (arb. units)

To avoid GPE local minima only enough strain is extracted so that the resulting *strain heating* is limited to a value just below the adlayer melting points. This maximises the chances of the system evolving towards a global minimum PE configuration. One could argue that if the temperature of the system was raised to the same level, to just below the melting point, by scaling up the velocities that an equivalent sampling of configuration space would be achieved. In practice the pres-

ence of initial strain, ie. non-ideal initial positions, proved more effective in achieving a lower final GPE than did any heating of the system to a comparable initial state. Hence it was important that the strain reducing program, `BEST_Zs`, did not reduce the GPE excessively.

2.5.4 Initial velocities

The initial velocity of each particle determines the starting temperature of the system. Taking into account that there will be *strain-heating*, the setting of an initial temperature by assigning initial velocities becomes a second determinant of the overall temperature. As mentioned in the previous section the equilibrium temperature should level out at a value below that which would cause the adlayer to melt. The exact adlayer melting point varies with the different adlayer reconstructions [6]. The temperature of a system of N moveable atoms is determined from :

$$\frac{3}{2}Nk_bT = \sum_{i=1}^{N}\frac{1}{2}m_iv_i^2 \tag{11}$$

where

v = velocity magnitude of particle i

m = mass of particle i

N = number of moveable particles

T = system temperature

k_b = Boltzmanns constant

The individual velocities in a real sytem vary according to a Maxwell-Boltzmann (*MB*) distribution with the systems *Temperature* corresponding to the average kinetic energy over all N atoms (equation 11). Ideally one would think that the initial velocity magnitudes should be assigned according to a *MB* distribution however there is no need since any initial velocity distribution will quickly approach a Maxwell-Boltzmann distribution as temperature equilibrium is reached. The initial distribution used is simply a delta function with every particle assigned the same kinetic energy hence resulting in an identical average kinetic energy for the complete

system. This simplifies velocity allocation when a particular initial temperature is required. With a specified temperature T, the particle velocity magnitudes are found from equation (11) above. Since every particle receives the same kinetic energy, equation (11) becomes :

$$\frac{3}{2}Nk_bT = \frac{1}{2}Nm_iv_i^2$$

yielding the velocity magnitude :

$$v_i = \sqrt{3k_bT/m_i} \tag{12}$$

Using equation (12), velocity magnitudes were computed for both the copper and lead atoms.

The velocity magnitudes must be split into the component velocities v_x, v_y and v_z. Component velocities are allowed positive and negative values thus enabling movement in both directions along a component axis. The velocity magnitude v is related to its components by :

$$v = \sqrt{v_x^2 + v_y^2 + v_z^2} \tag{13}$$

The directions and actual amplitudes of the component velocities are assigned randomly as described below while satisfying equation (13). Using two random numbers r_1 and r_2 $(0 \leq r_1, r_2 \leq 1)$ and a velocity magnitude $\mathbf{v}$, component velocities were assigned as follows :

$$\begin{aligned} v_x^2 &= r_1 \times \mathbf{v}^2 \\ v_y^2 &= (1 - r_1) \times r_2 \times \mathbf{v}^2 \\ v_z^2 &= (1 - r_1) \times (1 - r_2) \times \mathbf{v}^2 \end{aligned}$$

This ensures that $\mathbf{v}^2$ is randomly split among v_x^2, v_y^2 and v_z^2 in the ratio

$$r_1 \quad : \quad r_2 \quad : \quad 1 - r_1 - r_2$$

while satisfying equation (13). Random directions are achieved simply by multiplying the component velocities by a random number that is either $+1$ or -1.

After the initial velocities have been set there is a non-zero net momentum in each of the component directions. This momentum must be reset to zero so as to prevent any possible flow of particles accross the periodic boundaries or any spurious effects caused as a result of having a fixed zero momentum bottom layer and non-zero momentum in the upper layers.

In order to reset the total momentum to zero the total momentum in each direction P_x, P_y and P_z must be calculated using a sum over every moveable particle, ie.

$$P_\gamma = \sum_i^N m_i \times v_i^\gamma$$

The subscript γ represents any of the three component directions. The value N in this case is the total number of moveable particles. The total excess component momentum, P_γ, divided by the number of moveable particles N, corresponds to the excess momentum per atom. This quantity is labeled p_γ.

$$p_\gamma = P_\gamma / N$$

This excess momentum per atom is subtracted from the momenta of each particle. This simply means a loop over every moveable particle i and subtracting the excess momentum, ie.

$$v_i^\gamma = v_i^\gamma - p_\gamma / m_i$$

The resulting velocity adjustments mean that the initial temperature will have been affected. To regain the correct initial temperature the component velocities are scaled accordingly. This final scaling of the velocities has no effect on the net momentum which remains zero.

2.5.5 Initial accelerations

The initial acceleration components a_x, a_y and a_z are determined according to the initial positions explained in section 2.5.2. The acceleration components can be calculated independently since the force on an atom can be resolved into the three

component directions. The superposition of the component forces result in a net force on the atom. The acceleration of particle i in the γ direction is related to the net force on it, f_i^γ, in that direction by :

$$f_i^\gamma = m_i a_i^\gamma \tag{14}$$

where

f_i^γ = net γ component force on particle i
m_i = mass of particle i
a_i^γ = net γ component acceleration of particle i

The net force on particle i is determined by its interaction with its neighbours. Specifically those nearest-neighbours that are within a given *cut-off radius*, r_c , of the particle itself. Neighbours within this sphere are the only particles considered when calculating the net force on particle i, which is at the centre of the sphere. As will be explained Chapter 3, the larger the *atom-atom* separation the less force they exert on each other. The potential energy of one particle in an atom-atom interaction is given by the particular potential energy (PE) function used.

As mentioned in Section 2.3, the force on an atom is due only to those particles listed in its neighbour list. Therefore the force calculation, which results in the component net accelerations, simply involves a set of two loops. The first loop steps through the indices of each of the moving particles in the lattice while the second internal loop steps through the indices of every neighbour of a particular particle. Each neighbour contributes to a net acceleration, which is summed in this internal loop. The following loop structure is used to evaluate the net *two-body* forces on every particle due to the neighbours listed in their respective neighbour lists.

Loop ($i = 0$ **To** `NumParticles`) {

Loop ($Nebr = 0$ **To** `NumNebrs`) {

Calculate force on particle i due to the $Nebr$ particle.

}

}

The *Erkoς* force calculation requires an extra internal loop in order to evaluate the *three-body* contributions to the net force. The two outer loops are identical to those explained above. The third loop, which is the innermost loop, is needed to step through the indices of every neighbour in the particles neighbour list while avoiding identical neighbours and identical neighbour-neighbour pairs. The following loop combination ensures that every pair of neighbours is considered once at most.

Loop ($i = 0$ **To** `NumParticles`) {

Loop ($FirstNebr = 0$ **To** (`NumNebrs` -1)) {

Loop ($SecondNebr = (FirstNebr + 1)$ **To** `NumNebrs`) {

Calculate force on particle i due to $firstNebr$-$SecondNebr$ pair.

}

}

}

Using this loop structure the pair combinations are produced when needed avoiding the necessity to store combinations of neighbour pairs explicitly.

2.6 Program Flow

In this section the program flow is explained. The sequence of operations will be given, each main operation having been explained in earlier sections of this Chapter.

Some of the main preset values set at the beginning of the simulation include :

`Temperature`	Temperature in degrees Kelvin
`NUMSTEPS`	Number of time steps
`TIMESTEP`	Actual reduced time step value

`MAXNUMPARTICLES`	Maximum number of particles
`NumParticles`	Actual number of particles
`NUMLEADATOMS`	Number of adlayer atoms
`Nebr_R`	Neighbour List cut-off radius, r_c
`Nebr_dR`	Neighbour List outer shell width, Δr_c

Initially the reduced mass values of copper and lead are set, ie.

$$\texttt{Mass[CU]} = 63.546 \text{ amu}$$
$$\texttt{Mass[PB]} = 207.200 \text{ amu}$$

The parameters for the particular potential being used are then read in from a file. The initial velocities are then set as described in Section 2.5.4. The initial positions described in Section 2.5.2 are then allocated. The z values are read in from a file created by the `BEST_Zs` program as explained in Section 2.5.3. To ensure that there is no net flow of particles with respect to the fixed layer, the net momentum is set to zero as detailed in Section 2.5.4. The moveable particle's neighbour lists are then constructed, this is explained in Section 2.3. The acceleration components are initialised using the newly created neighbour lists as described in Sections 2.5.5. At this point all simulation initialisation is complete.

A *time-loop* is now required to step the system forward in time. The *Verlet* algorithm allows successive coordinates and velocities to be calculated at each time step. The force expressions given in Chapter 3, sections 3.5.1 and 3.5.2, are used to evaluate the component forces at each time step. These acceleration values are then used in the Verlet function to update positions and velocities according to Section 2.4. The essential operations repeated in the time loop are given below.

1. The summed maximum displacement variable, initialised at zero, is checked with respect to the neighbour-listing criteria given in Section 2.3. According to the value of this variable the neighbour lists may need to be rebuilt.

2. The Verlet function updates the particle coordinates and velocities by combining formula (5) and (6) given in Section 2.4 with the results of the force

function which calculates the net component forces on each atom. Note that the Verlet velocity formula involves successive (in time) acceleration components which means that the force function needs to be called in the 'middle' of the Verlet adjustment. New coordinates in the x and y directions are subjected to *Periodic Boundary Conditions* as explained in Section 2.2.1. The kinetic energy is also calculated on exiting the Verlet function which will be used to give the temperature of the system at that particular timestep. The time variable is incremented by the value of the time step.

3. Finally the `Properties` function is called which calculates the instantaneous temperature, the temperature at that time step, as well as an average of the temperature. The instantaneous temperature versus time data is also printed to a file.

On exiting the time-loop the coordinates of every particle are printed to a file for analysis. A flow chart of the program is given in Fig. 2.7 below.

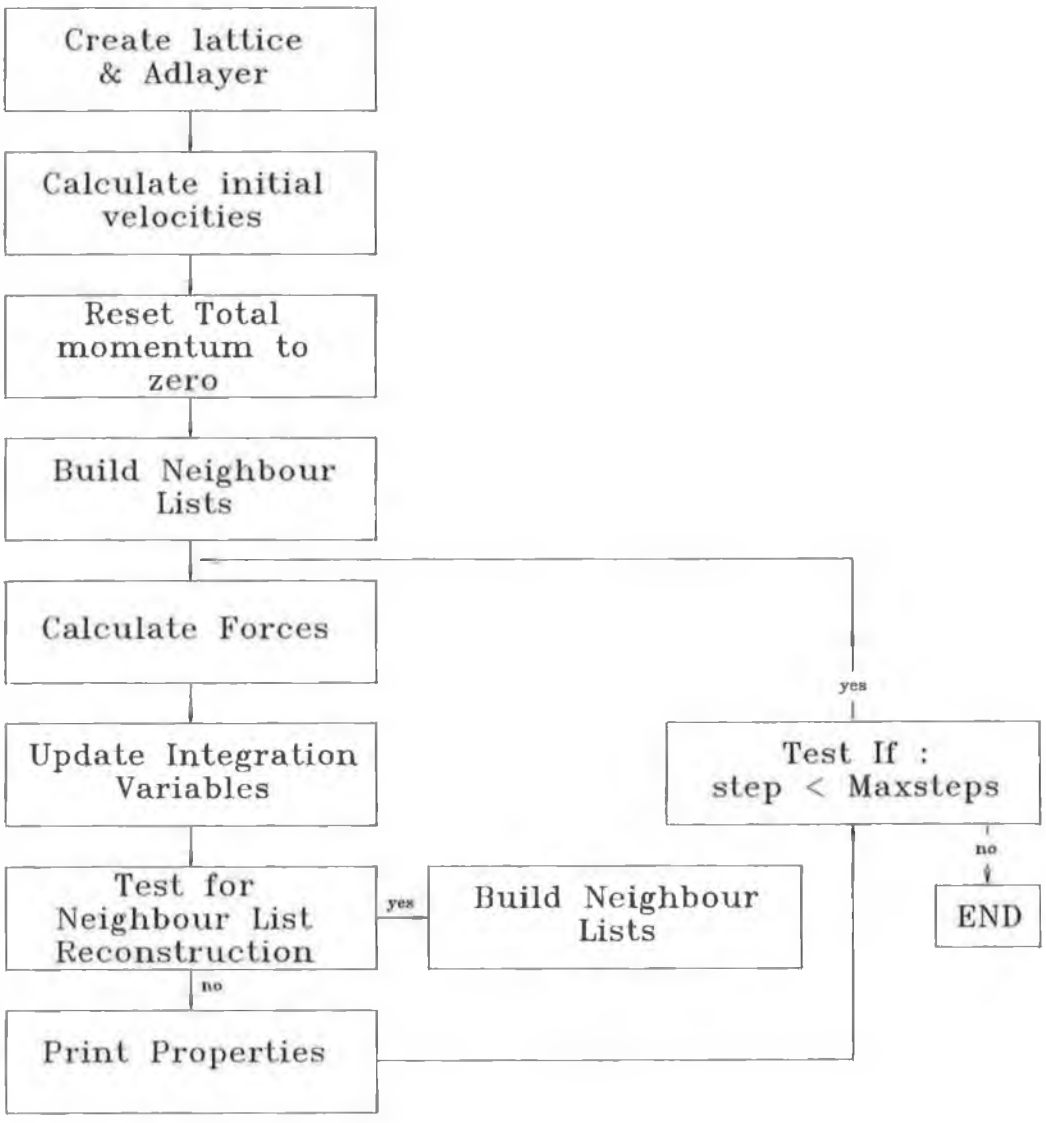

Figure 2.7: MD flow diagram.

Chapter 3 Theory

3.1 Introduction

The first section of this chapter describes the three different superstructures that form when sub-monolayer coverages of lead are deposited on the (100) face of copper. In order of increasing coverage the three structures are as follows:

structure	coverage
c(4×4)	0.375
c(2×2)	0.5
c($5\sqrt{2} \times \sqrt{2}$)R45°	0.6

The exact details of the c(2×2) and c($5\sqrt{2} \times \sqrt{2}$)R45° superstructures are well established. The exact structure of the c(4×4) however is less obvious and has been the subject of much study in recent years.

In section 3.5 the potential energy functions (PEF) are given. The corresponding force expressions are also presented. In the case of the Lennard-Jones potential a full derivation of the force expression is given. The *Erkoς* derivation for the force can be found in Appendix A.

3.2 The c(4×4) structure

Based on Auger electron spectroscopy (AES) a chain model was proposed for the structure of the c(4×4) reconstruction [**2**]. This model became especially plausable after the tendency of lead atoms to form chains leading to one-dimensional epitaxy was demonstrated by Dreschler[**8**]. The chain model consists of parallel chains of lead atoms with adjacent chains separated by a distance of $\sqrt{2}$ times the lattice constant along a chain, as shown in Fig. 3.8. The channels between the lead chains are unoccupied.

In an STM study [**3**], a surface alloy model was proposed for the c(4×4) reconstruction, despite the fact that lead and copper are immiscible in the bulk. A

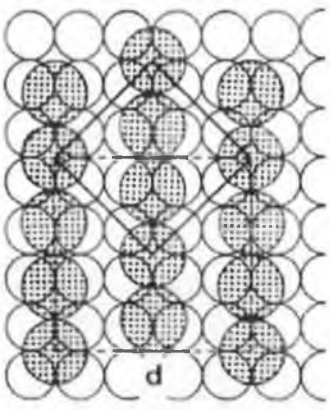

Figure 3.8: c(4×4) hollow chain model **[2]**

new model was put forward where the corner atoms of the c(4×4) unit cell were situated on bridge sites. This would result in every third lead atom along a chain to be slightly raised. This was indeed observed as can be seen from the STM image in figure 3.9 below. It was noted that at coverages above $\Theta = 0.375$ copper islands formed which indicated a dealloying of the c(4×4) structure.

The formation of a surface alloy would require lead atoms to be embedded into the copper substrate. Evidence for the embedding of lead was found **[3]** at very low coverages ($\Theta = 0.03$). The STM image obtained, figure 3.10 below, shows various bright spots which remain stable and visible for up to a few minutes implying that they were lodged in the surface and embedded. The height of the lead atom was found to be $0.6\mathring{A}$ which is much less than the substrate inter-layer spacing, thus indicating that the lead was embedded. A low energy electron spectroscopy (LEED) `I/V` calculation was undertaken **[4]** to determine the most probable structure for the c(4×4) reconstruction. Three `R-factors` ,R_p, R_{ZJ} and R_{DE} were used to evaluate a particular model. The lower the value of the respective `R-factors` for a model the better the comparison between the model `I/V` curves and the experimental ones. Three different models were considered, the vacancy model, the chain model and the alloy model. Based on STM results the vacancy model was discarded. Figure 3.11 shows both the chain and alloy models including corner atoms situated on both the hollow and bridge sites.

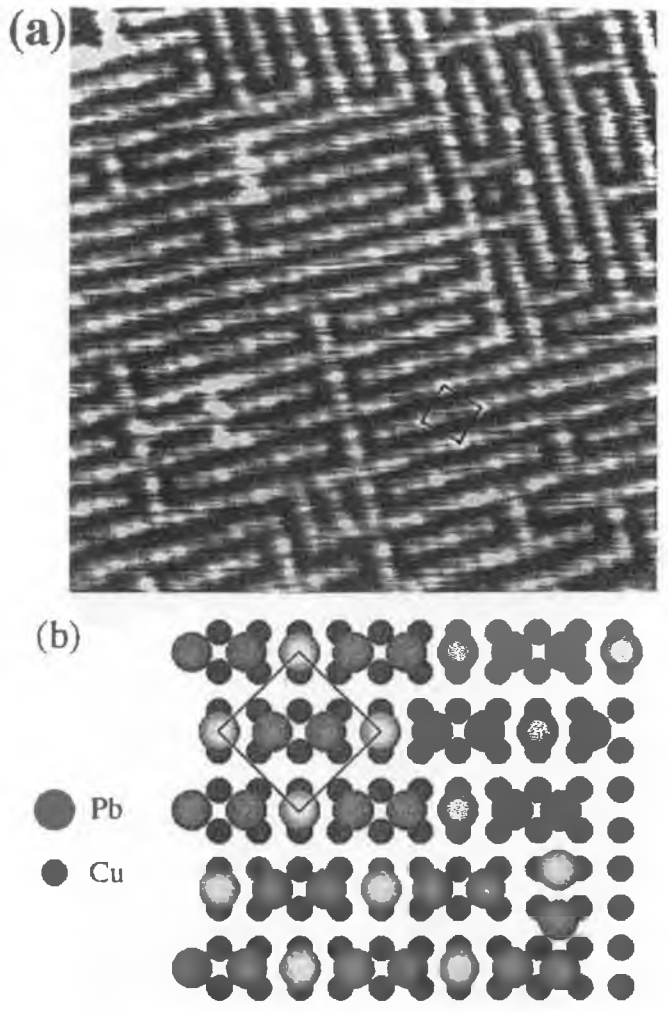

Figure 3.9: c(4×4) bridge alloy STM and model [3]

With the chain model the Pb-Pb separation is 3% less than that found in bulk lead. Inter-chain distance (5.112Å) is much larger than the atom-atom separation (3.408Å) along a chain for equally spaced atoms

One explanation for the inter-chain spacing lies in the possibility of surface alloying suggested by the STM study of Pb on Cu(111) [9].

The initial atom positions for the alloy calculations involved copper atoms taking on bulk-like positions but with the possibility of lateral and vertical relaxation to avoid unrealistic Cu-Pb or Cu-Cu separations. The presence of copper chains makes any zig-zag displacement of Pb atoms quite unlikely. Longitudinal displacements of lead atoms are allowed. The results of the LEED I/V calculation are given below.

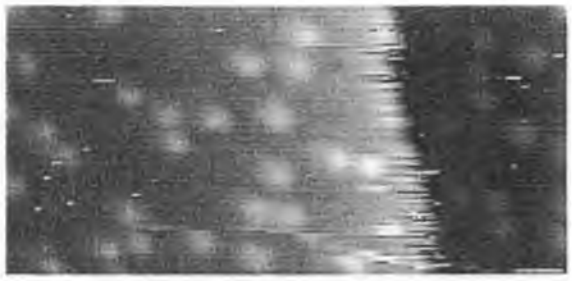

Figure 3.10: Embedded lead on copper (100) **[3]**

MODEL	R_{DE}	R_P
chain model (bridge sites)	0.530	0.708
chain model (hollow sites)	0.519	0.599
alloy model (bridge sites)	0.492	0.528
alloy model (hollow sites)	0.347	0.307

From the table it is clear that the hollow sites for the corner atoms of the unit cell were favoured over the bridge sites for both the chain and alloy models. The hollow site alloy model agrees most closely with experimental I/V curves yielding the lowest set of R-factors. A diagram of the exact positions of the hollow site alloy model atom positions is shown in figure 3.12 below. The diagram shows lead chains with adjacent chains differing by a distance along a chain of $\sqrt{2}$ times the lattice constant. Also the copper chains, which are between lead chains, are modulated with a periodicity of approximately 8 atoms. The exact details of this modulation were examined in the current study, the results of which are presented in chapter 4. The details of the displacements in the z direction are also given.

The STM study by Nagl et al **[3]** suggests that unit cell corner atoms lie on bridge sites. There is a clear contradiction with the LEED study **[4]**.

A further STM study **[5]** was undertaken which revealed more evidence that the c(4×4) reconstruction is a surface alloy. It was noted that in a given region $52 \pm 5\%$ of the area was occupied by a monotatomic copper step while the rest was c(4×4). The simplest interpretation is that a surface alloy of Pb_3Cu_4 is formed which would account for the migration of half a copper layer leading to the formation of a c(4×4)

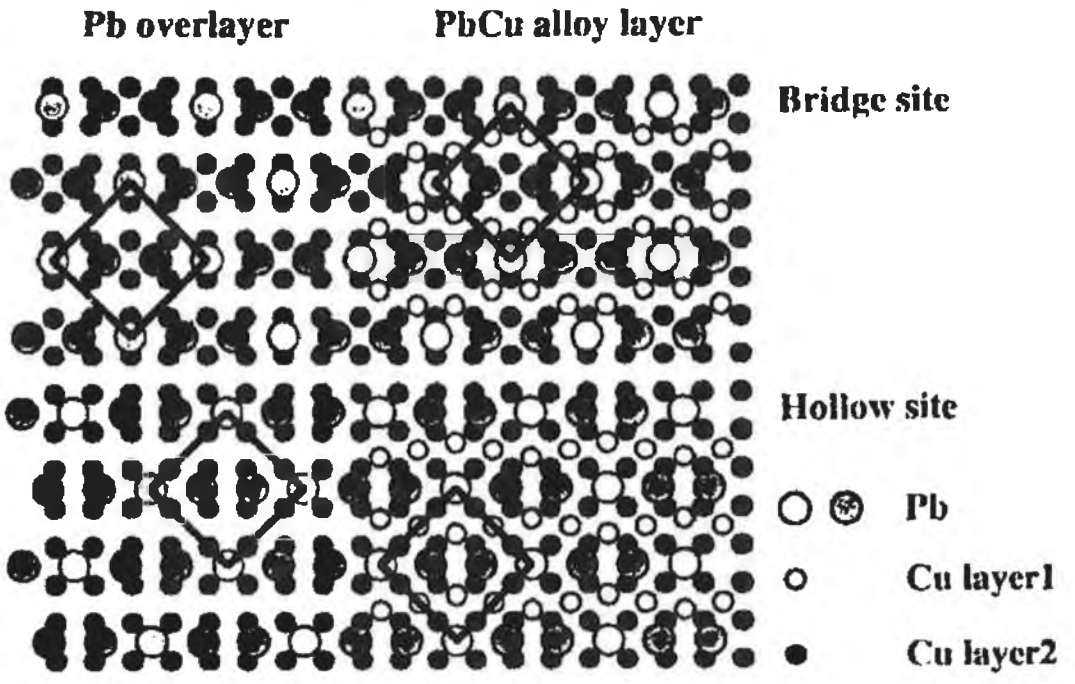

Fig. 3. Left site: chain model in hollow and bridge site. Right side: CuPb alloy layer, Pb in the bridge and in the hollow sites.

Figure 3.11: c(4×4) chain and alloy models [4]

alloy domain and a copper step. The alloy model was thus asserted.

A Monte Carlo simulation [6] revealed, in agreement with Gauthier et al [4] figure 2.4, that a modulation of copper atoms occurs with a periodicity of approximately 8 atoms.

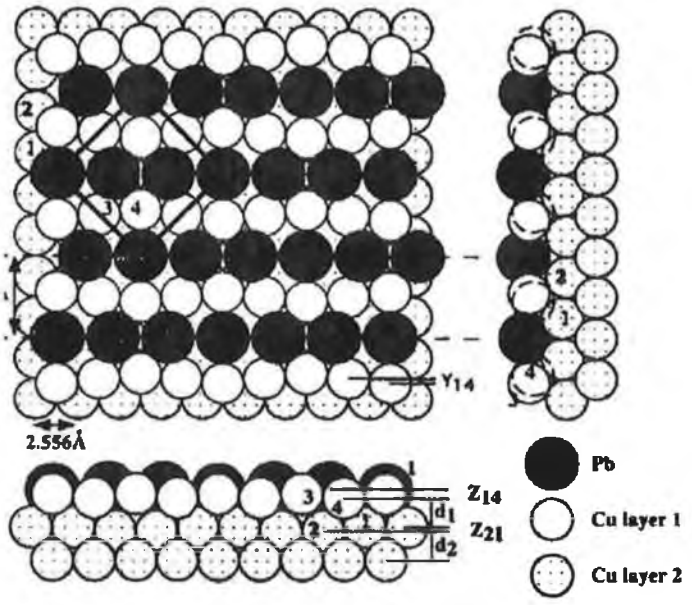

Figure 3.12: c(4×4) hollow alloy model with copper modulation [4]

3.3 The c(2×2) structure

The c(2×2) structure forms at a coverage of $\Theta = 0.5$. The exact structure is well established but is given for completeness. Figure 3.13 below shows the exact form of the c(2×2) superstructure. The c(2×2) reconstruction is a common structure for the deposition of a metal on the (100) face of copper [11], [12].

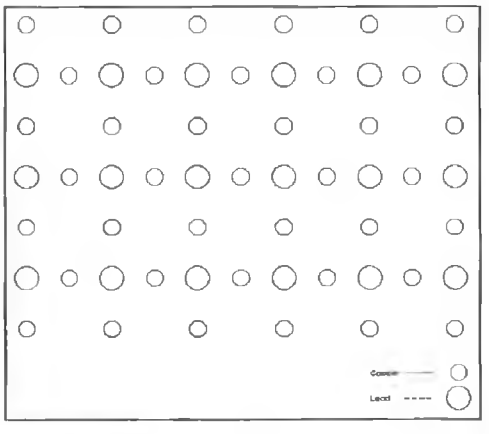

Figure 3.13: c(2×2) reconstruction

3.4 The c($5\sqrt{2} \times \sqrt{2}$)R45° structure

The earliest model for the c($5\sqrt{2} \times \sqrt{2}$)R45° structure [1] is shown in figure 3.14. This model assumes a uniform hexagonal lead overlayer. The c($5\sqrt{2} \times \sqrt{2}$)R45°

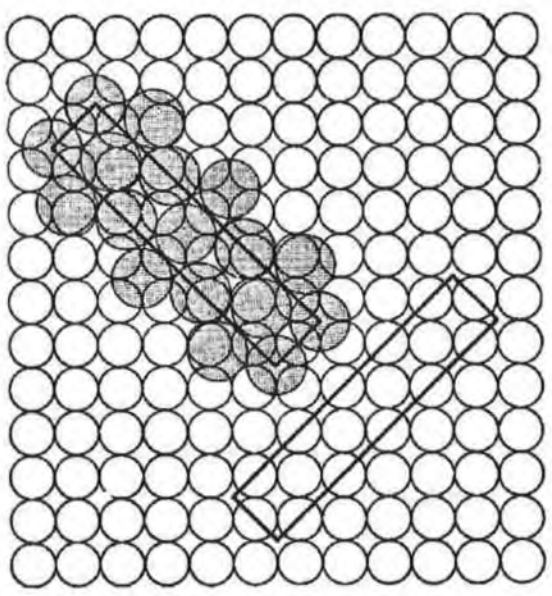

Figure 3.14: Henrion and Rhead c($5\sqrt{2} \times \sqrt{2}$)R45° model [1]

structure forms at a coverage of $\Theta = 0.6$. At the lower coverage of $\Theta = 0.5$ the c(2×2) superstructure forms. As the coverage is increased from $\Theta = 0.5$ it is proposed that anti-phase boundaries are inserted into the c(2×2) structure [3]. At $\Theta = 0.6$ the anti-phase boundaries are equally spaced with three rows of the c(2×2) structure being separated by anti-phase domain boundaries. The STM image, shown in figure 3.15, obtained by Nagl et al [3] confirms the anti-phase domain boundary model. A diagram of the anti-phase model for the c($5\sqrt{2} \times \sqrt{2}$)R45° structure [5] is given in figure 3.16.

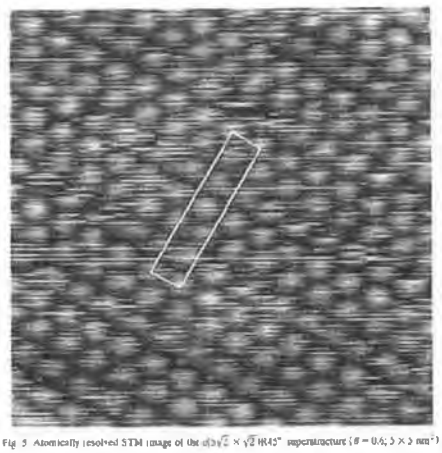

Figure 3.15: c($5\sqrt{2} \times \sqrt{2}$)R45° STM result [3]

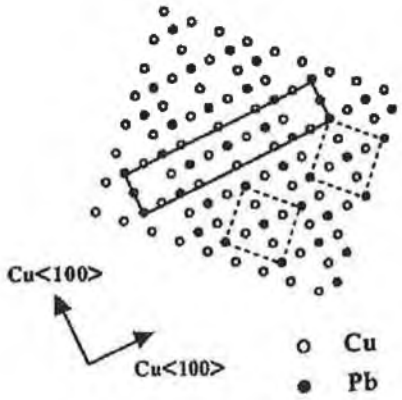

Figure 3.16: Anti-phase domain boundary model [5]

3.5 Description of potentials

Two potential energy functions are used in the current project. The first function is a two-body Lennard-Jones potential [6]. The second is a three-body *Erkoς* potential [7]. The force on a particle is found by differentiating the respective potential energy function (PEF) with respect to position. In mathematical terms the force on a particle is the negative of the gradient of the PEF, ie.

$$\vec{\mathbf{f}} = -\nabla V$$

$$\vec{\mathbf{f}} = -\frac{\partial V}{\partial x}\vec{\mathbf{i}} - \frac{\partial V}{\partial y}\vec{\mathbf{j}} - \frac{\partial V}{\partial z}\vec{\mathbf{k}}$$

where

$\mathbf{f}$ = force
V = Potential energy function
x, y, z = component directions
$\vec{\mathbf{i}}, \vec{\mathbf{j}}, \vec{\mathbf{k}}$ = unit vectors

The total force on a particle is due to the interaction with all other particles in the region thus the gradient must be computed for each of the surrounding particles.

3.5.1 Lennard-Jones potential energy function

The Lennard-Jones (LJ) PEF is given [6] by the expression,

$$V_{ij} = \frac{\epsilon}{n-1}\left\{\frac{\sigma^{mn}}{r_{ij}^{mn}} - n\frac{\sigma^{m}}{r_{ij}^{m}}\right\} \tag{15}$$

where

ϵ = potential energy well depth
σ = characteristic distance for PEF
n, m= numerical variable exponents
r_{ij} = separation of particles i and j

Equation (15) gives the potential energy of particle i due to particle j. The distance between the two particles, r_{ij} is calculated using,

$$r_{ij} = \sqrt{(x_i - x_j)^2 + (y_i - y_j)^2 + (z_i - z_j)^2}$$

or

$$r_{ij} = \sqrt{\Delta x_{ij}^2 + \Delta y_{ij}^2 + \Delta z_{ij}^2}$$

where

$$\Delta x_{ij} = x_i - x_j \quad \text{... etc.}$$

The force on particle i due to particle j is labeled $\mathbf{f}_{ij}$. The force becomes,

$$\mathbf{f}_{ij} = -\frac{\partial V_{ij}}{\partial x}\vec{\mathbf{i}} - \frac{\partial V_{ij}}{\partial y}\vec{\mathbf{j}} - \frac{\partial V_{ij}}{\partial z}\vec{\mathbf{k}} \tag{16}$$

If r^γ is to represent x, y or z, then the derivative $\partial V_{ij}/\partial r_i^\gamma$ is a general form for the partial derivatives in (16). For $r_i^\gamma = x_i$, then $\Delta r_{ij}^\gamma = x_i - x_j$.

The LJ PEF can be written as,

$$V_{ij} = \frac{\epsilon}{n-1}\left\{\sigma^{mn} r_{ij}^{-mn} - n\sigma^m r_{ij}^{-m}\right\}$$

Differentiating this expression with respect to r_i^γ we get,

$$\frac{\partial V_{ij}}{\partial r_i^\gamma} = \frac{\epsilon}{n-1}\left\{-mn\sigma^{mn} r_{ij}^{-mn-1}\frac{\partial r_{ij}}{\partial r_i^\gamma} + mn\sigma^m r_{ij}^{-m-1}\frac{\partial r_{ij}}{\partial r_i^\gamma}\right\} \tag{17}$$

We now need $\partial r_{ij}/\partial r_i^\gamma$. Taking $r_i^\gamma = x_i$ then,

$$r_{ij} = \sqrt{(x_i - x_j)^2 + (y_i - y_j)^2 + (z_i - z_j)^2}$$

The derivative with respect to x_i becomes,

$$\frac{\partial r_{ij}}{\partial x_i} = \frac{x_i - x_j}{\sqrt{(x_i - x_j)^2 + (y_i - y_j)^2 + (z_i - z_j)^2}}$$

or in general,

$$\frac{\partial r_{ij}}{\partial r_i^\gamma} = \frac{\Delta r_{ij}^\gamma}{r_{ij}} \tag{18}$$

Substituting back into (17) we get,

$$\frac{\partial V_{ij}}{\partial r_i^\gamma} = \frac{\epsilon}{n-1}\left\{\frac{-mn\sigma^{mn}}{r_{ij}^{mn+2}}\Delta r_{ij}^\gamma + \frac{mn\sigma^m}{r_{ij}^{m+2}}\Delta r_{ij}^\gamma\right\}$$

which reduces to,

$$\frac{\partial V_{ij}}{\partial r_i^\gamma} = \frac{mn\epsilon}{n-1}\left\{\frac{-\sigma^{mn}}{r_{ij}^{mn}} + \frac{\sigma^m}{r_{ij}^m}\right\}\frac{\Delta r_{ij}^\gamma}{r_{ij}^2}$$

The force on particle i due to particle j in the γ direction, $\mathbf{f}_{ij}^\gamma$, is given by,

$$\mathbf{f}_{ij}^\gamma = \frac{mn\epsilon}{n-1}\left\{\frac{\sigma^{mn}}{r_{ij}^{mn}} - \frac{\sigma^m}{r_{ij}^m}\right\}\frac{\Delta r_{ij}^\gamma}{r_{ij}^2} \tag{19}$$

The x component, for example, of the force would be,

$$\mathbf{f}_{ij}^x = -\frac{\partial V_{ij}}{\partial x_i} = \frac{mn\epsilon}{n-1}\left\{\frac{\sigma^{mn}}{r_{ij}^{mn}} - \frac{\sigma^m}{r_{ij}^m}\right\}\frac{x_i - x_j}{r_{ij}^2}$$

Using expression (19) the net component force, $\mathbf{F}_i^\gamma$, on any particle i, can be evaluated using a computational loop over all j particles ie.

$$\mathbf{F}_i^\gamma = \sum_{j:j\neq i}^{N} \mathbf{f}_{ij}^\gamma \tag{20}$$

where N is the total number of particles in the region. Expression (20) was used in the simulation to evaluate the net component force $\mathbf{F}_i^\gamma$, on each particle for the Lennard-Jones potential. The necessary parameters for the Lead-Copper system are given in the table below **[6]**.

	m	n	ϵ(eV)	σ(Å)
CU-CU	5	1.1	0.22405	2.7386
CU-PB	5	1.25	0.1877539	3.176776
PB-PB	5	1.4	0.1572831	3.615

Figure 3.17 below shows a plot of the Cu-Cu potential energy function.

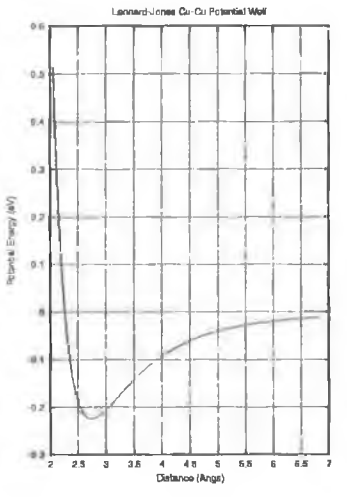

Figure 3.17: Lennard-Jones PEF for Cu-Cu

3.5.2 *Erkoς* potential energy function

The *Erkoς* potential [7] is a three-body potential. This means that when calculating the force on a particle i, all pairs of atoms (j and k) must be considered while excluding particle i. The expression which gives the potential energy of a particle i due to particles j and k is given by,

$$V_{i,jk} = U_{ij} + U_{ik} + C_3 U_{ij} f_{ijk} + C_3 U_{ik} f_{ikj} + C_3 U_{jk} f_{jki} \tag{21}$$

where

$$U_{ij} = C_2 A \left\{ \frac{r_0^{2n}}{r_{ij}^{2n}} \exp(-2\alpha \frac{r_{ij}^2}{r_0^2}) \; - \; \frac{r_0^n}{r_{ij}^n} \exp(-\alpha \frac{r_{ij}^2}{r_0^2}) \right\}$$

and

$$f_{ijk} = \exp(-\frac{r_{ik}^2 + r_{jk}^2}{r_0^2})$$

The force on particle i due to particles j and k is found by differentiating (21) with respect to x, y or z. If r^γ denotes x, y or z then the force expression $\mathbf{f}_{i,jk}^\gamma$ is given by,

$$\mathbf{f}_{i,jk}^\gamma \;=\; C_2 A \Delta r_{ij}^\gamma \omega_{ij} \tau_{ij} (2\tau_{ij} - 1) \; + \; C_2 A \Delta r_{ik}^\gamma \omega_{ik} \tau_{ik} (2\tau_{ik} - 1)$$

$$+ \quad C_3C_2Af_{ijk}\tau_{ij}\left\{\frac{2\Delta r_{ik}^{\gamma}}{r_0^2}(\tau_{ij}-1) + \Delta r_{ij}^{\gamma}\omega_{ij}(2\tau_{ij}-1)\right\}$$

$$+ \quad C_3C_2Af_{ijk}\tau_{ik}\left\{\frac{2\Delta r_{ij}^{\gamma}}{r_0^2}(\tau_{ik}-1) + \Delta r_{ik}^{\gamma}\omega_{ik}(2\tau_{ik}-1)\right\}$$

$$+ \quad 2C_3C_2Af_{jki}\tau_{jk}r_0^{-2}(\tau_{jk}-1)(\Delta r_{ij}^{\gamma}+\Delta r_{ik}^{\gamma}) \tag{22}$$

where

$$\begin{aligned}
\Delta r_{ab}^{\gamma} &= r_a^{\gamma} - r_b^{\gamma} \\
\omega_{ab} &= \frac{2\alpha}{r_0^2} + \frac{n}{r_{ab}^2} \\
\tau_{ab} &= r_0^n r_{ab}^{-n}\exp(-\alpha\frac{r_{ab}^2}{r_0^2}) \\
f_{abc} &= \exp(\frac{-r_{ac}^2 - r_{bc}^2}{r_0^2}) \\
\alpha &= \log_e(2)
\end{aligned}$$

Using expression (22) the component force $\mathbf{f}_{i,jk}^{\gamma}$ experienced by particle i due to particles j and k can be evaluated. This procedure is repeated for all pairs j and k resulting in a net component force, $\mathbf{F}_i^{\gamma}$,

$$\mathbf{F}_i^{\gamma} = \sum_{j,k\neq i}^{N} \mathbf{f}_{i,jk}^{\gamma} \tag{23}$$

where N is the total number of particles.

	C_2	C_3	A(eV)	$r_0(\mathring{A})$	n
CU-CU	0.1930176	-0.1261549	8.04	2.22	1.801698
CU-PB	0.3255652	-0.2657175	5.2284	2.575	2.612319
PB-PB	0.4581129	-0.4052801	3.4	2.93	3.422940

The parameters of the Erkoς potential for the Lead-Copper system are given in the table above.

Figure 3.18 below shows a plot of the two-body part of the Erkoς potential.

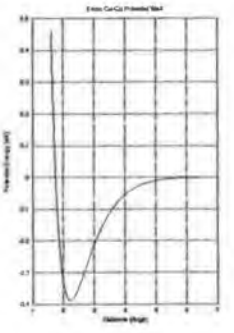

Figure 3.18: Erkoc PEF for Cu-Cu

Chapter 4 Results and Conclusions

In this Chapter the results of the current Molecular Dynamics simulation of the deposition of Pb on the (100) face of Copper are presented. The three possible reconstructions, c(4×4), c(2×2) and c($5\sqrt{2} \times \sqrt{2}$)R45° are considered using both the Lennard-Jones [6] and Erkoς [7] potentials.

4.1 The c(4×4) structure

This section contains the results of the MD simulation of the c(4×4) reconstruction, when modeled using both the two-body Lennard-Jones and three-body Erkoς potentials. The initial lead positions for every MD run of the c(4×4) structure was set to the hollow alloy model shown in figure 3.11. It was important that there was sufficient initial temperature in the system, while remaining below the overlayer melting point, to ensure effective sampling of configuration space, and thereby reducing the possibility of the system settling in a local minimum potential energy configuration. The alloy copper was deposited in a straight line along the troughs, in the hollow sites, between lead chains. There are four results presented, two results obtained using the Lennard-Jones potential and two results obtained using the Erkoς potential. The final positions of the alloyed copper atoms were also analysed.

4.1.1 Lennard-Jones c(4×4) MD results

In this section the results of the simulation of the c(4×4) reconstruction are given when modeled using the two-body Lennard-Jones potential energy function. The initial alloy configuration is identical to that shown in figure 3.11, the hollow alloy model. The corner atoms of the initial configuration are situated at hollow sites.

- **Lennard-Jones c(4×4) Result 1**

The $x-y$ coordinates of the initial alloy configuration were obtained from figure 3.11 with the alloy copper being deposited in straight lines. The z coordinates of the alloy layer proved more difficult to determine. At first a rough estimate was used for the alloy z values. The MD simulation was then started. On examination it was noted that the system temperature had risen to a value higher than the melting temperature (540K [6]) of the c(4×4) reconstruction. This heating of the system was due to excess strain in the crystal due to the initial z value approximation. In order to obtain a better approximation the 'bestZs' program, discussed in section 2.5.3 was used. Using this set of initial z values in the MD simulation the temperature of the system remained below the c(4×4) melting point.

Using an initial temperature of 0K the Molecular Dynamics simulation was started. The temperature rose and eventually reached an equilibrium temperature of 20K. The coordinates of the alloy and top substrate layers were processed so that the final configuration could be identified. Figure 4.19 below shows the first Lennard-Jones result for the c(4×4) reconstruction.

It can be seen that the hollow alloy model configuration remains. One possibility is that the hollow alloy model is the configuration that corresponds with the global potential energy minimum for the Lennard-Jones potential. Another possibility is that is that there was insuffucient kinetic energy in the system to sample configuration space adequately. In order to account for this possibility a scond MD simulation was run but with a starting temperature of 300K. The outcome of this run is given below as result number 2.

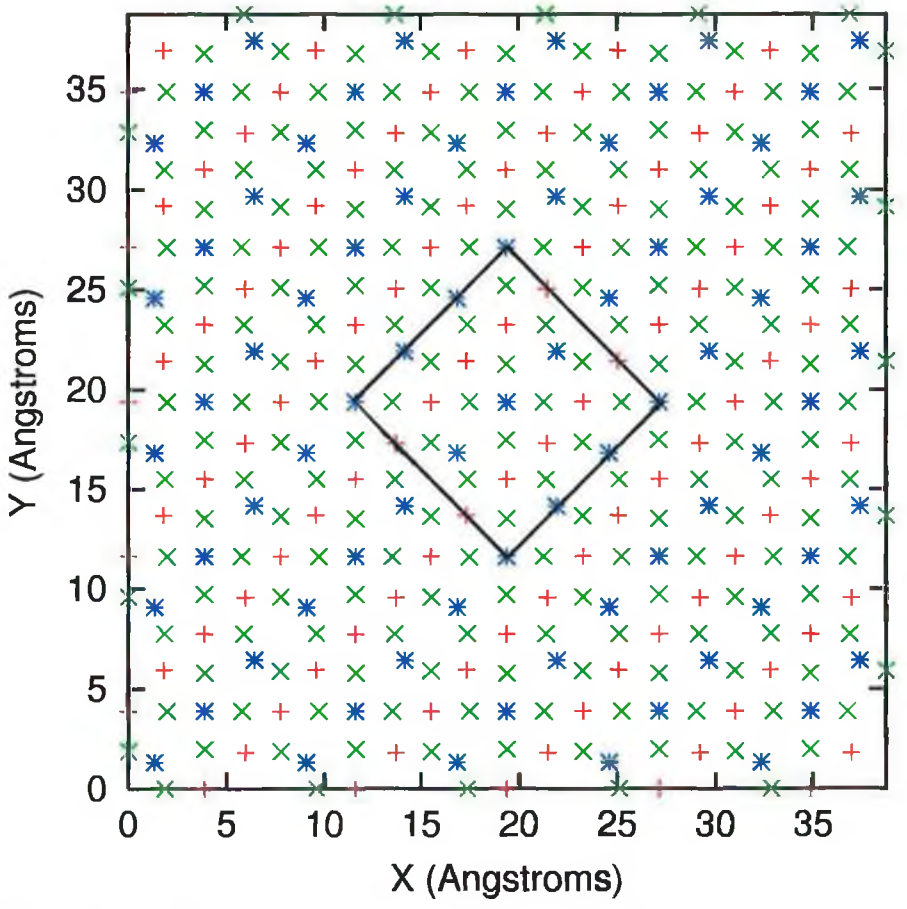

Figure 4.19: LJ result1 - c(4 × 4) reconstruction. Atoms marked green designate the uppermost copper substrate layer. Atoms marked red and blue represent the alloy copper and alloy lead respectively.

- **Lennard-Jones c(4 × 4) Result 2**

As mentioned above the initial temperature for this MD run was set to 300K. The initial configuration was set to the hollow alloy model. On completion of the MD run the alloy configuration was analysed with figure 4.20 below showing the resulting final configuration. A hard sphere 3D representation of this result is given below in figures 4.20a, 4.20b and 4.20c. These figures were produced using the SARCH software package of Van Hove **[13]**. The final configuration corresponds exactly with the bridge alloy model as shown in figure 3.11. The unit cell corner atoms lie on bridge sites as shown. Upon further analysis it was found that the lead atoms located at the bridge sites were slightly raised. Along any lead chain this gives consequetively two low atoms and one high atom, the high atom being the lead

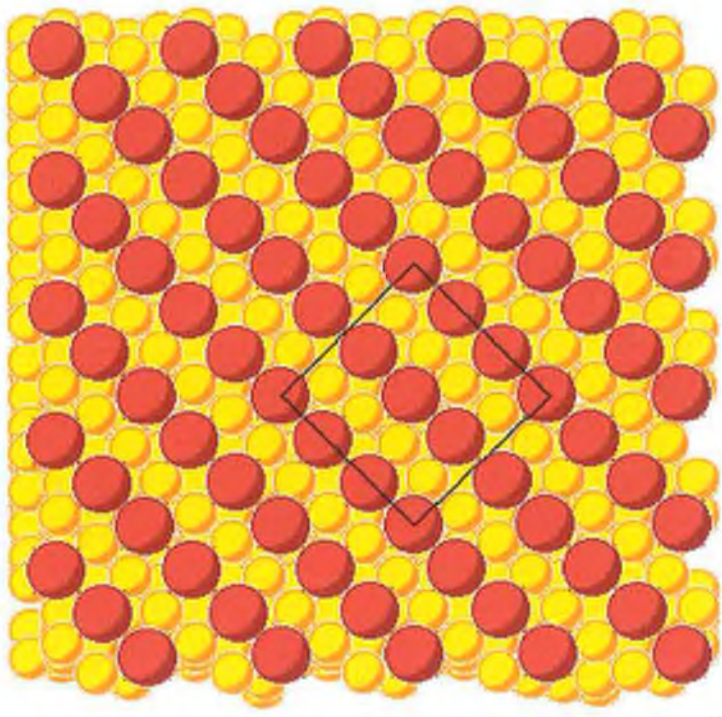

Figure 4.20a : c(4x4) reconstruction, face-on view with unit cell marked

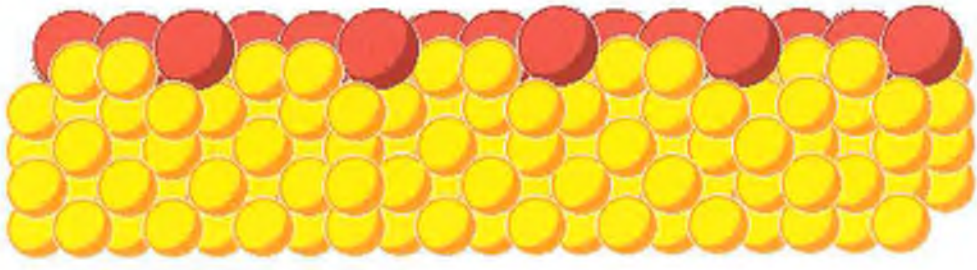

Figure 4.20b : c(4x4) reconstruction, side view

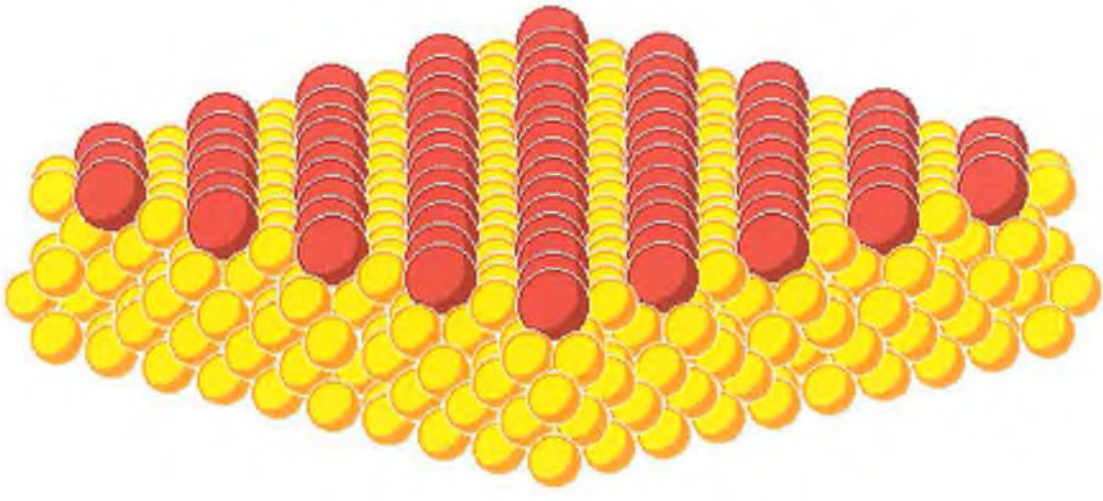

Figure 4.20c : c(4x4) reconstruction, edge-on view

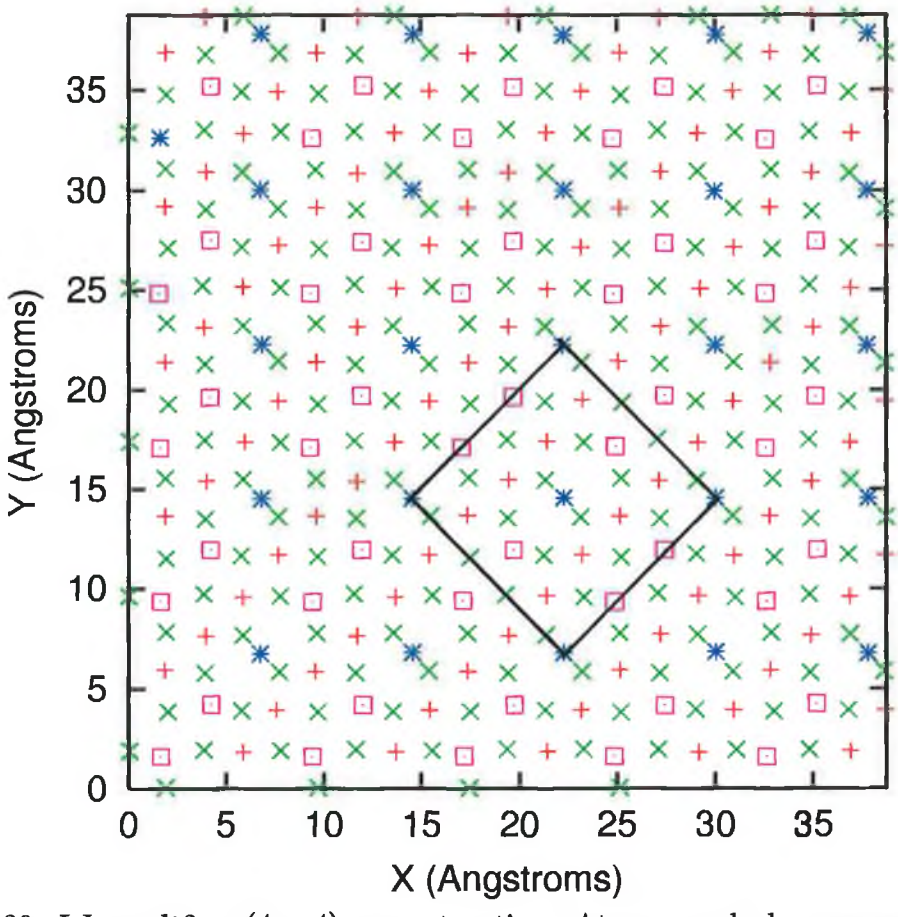

Figure 4.20: LJ result2 - c(4 × 4) reconstruction. Atoms marked green correspond to the uppermost copper substrate layer. Atoms marked red correspond to the alloy copper. Atoms marked blue and cyan correspond to alloy lead with blue atoms sitting at bridge sites

atoms situated on bridge sites. To demonstrate this more clearly a depth profile is given in figure 4.21 below. This figure shows that the alloy lead layer, labeled Pb-A, has split into two sub-peaks. It can be seen that there is a two to one ratio with the lead atoms located at the bridge sites corresponding to the lower fraction of the ratio. The separation between the Cu1 peak and the Cu-A peak was found to be 1.7±0.16Å. The separation between the Cu-A peak and the Pb-A peak (larger of two Pb sub-peaks) was found to be 0.82±0.13Å. The separation between the two Pb peaks (Pb-A) was found to be 0.12±0.06Å. This modulation in the z direction is in direct agreement with the STM study [**3**] of Nagl et al. The STM result shown in figure 3.9 clearly shows that every third atom is brighter or raised with respect

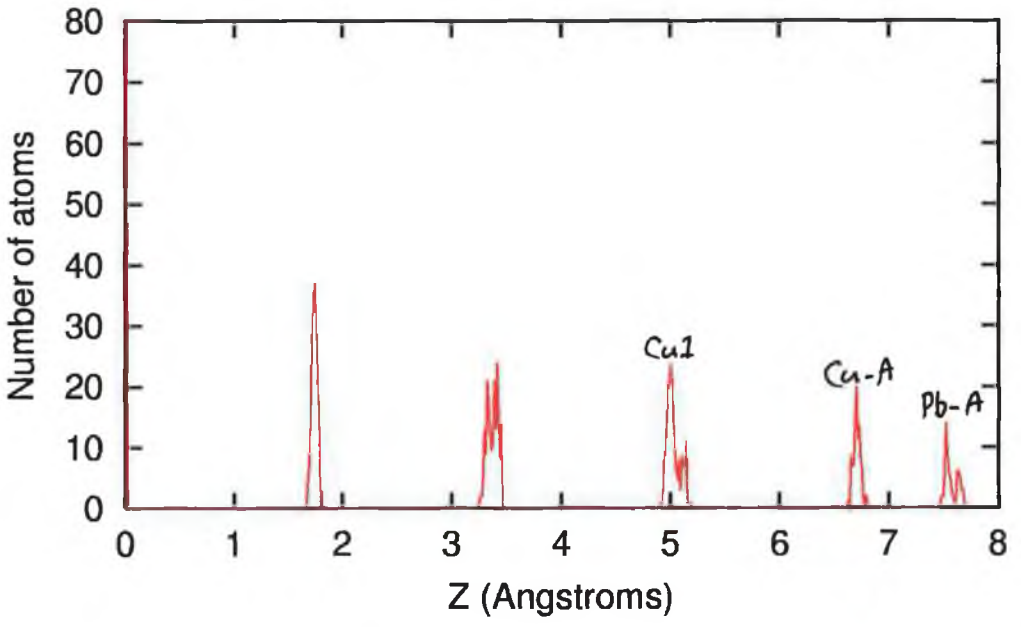

Figure 4.21: LJ result2 - c(4 × 4) z distribution. The alloy copper and alloy lead are labeled Cu-A and Pb-A respectively. The uppermost copper substrate layer is labeled Cu1.

to the lower or non-bright lead atoms.

The current Lennard-Jones MD simulation of the c(4 × 4) reconstruction clearly favours the bridge alloy model over the hollow alloy model. This is in disagreement with the I/V LEED study of Gauthier et al [4] in which it is concluded that the hollow alloy model is the likely structure for the c(4 × 4) reconstruction.

4.1.2 Erkoς c(4 × 4) MD results

In this section the results of the MD simulation of the c(4 × 4) reconstruction are given when modelled using the three-body Erkoς potential energy function. The initial configuration is that of the hollow alloy model as shown in figure 3.11. There are two results presented.

- **Erkoς c(4 × 4) Result 1**

The initial configuration was set to that of the hollow alloy model with unit cell corner atoms located at hollow sites. On completion of the MD run, after a

temperature rise of 30K from an initial temperature of 0K, figure 4.22 below resulted. From figure 4.22 it is clear that the final configuration is identical to the

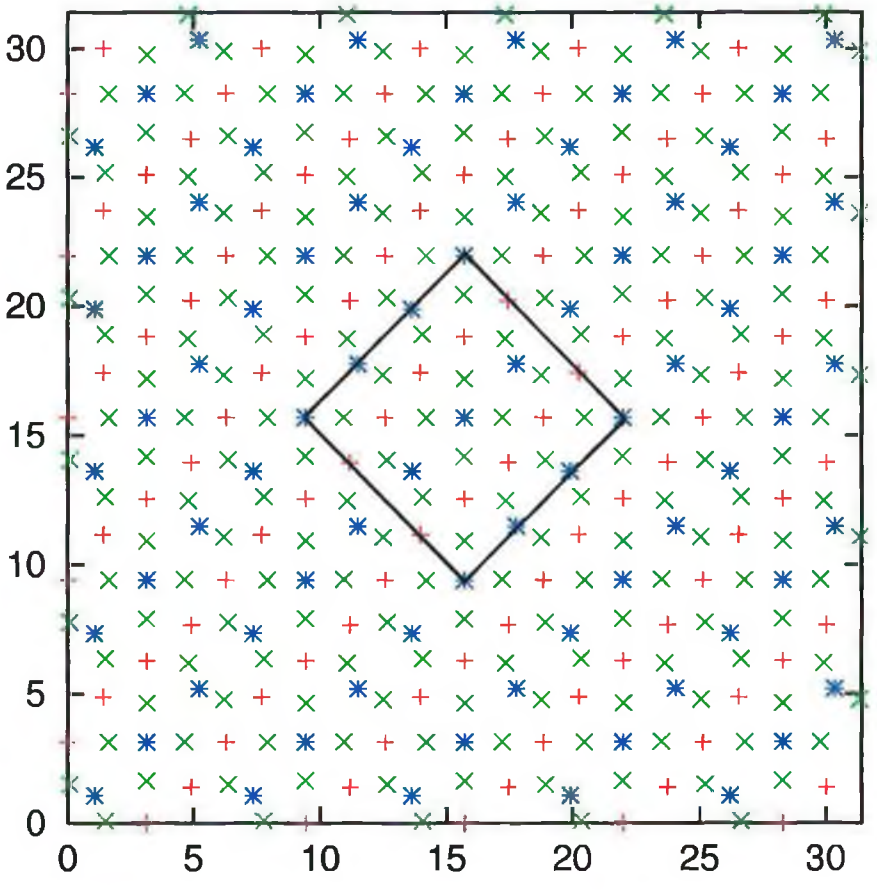

Figure 4.22: Erkoc result1 - c(4 × 4) reconstruction. Atoms marked green designate the uppermost copper substrate layer. Atoms marked red and blue represent the alloy copper and alloy lead respectively.

initial configuration. Two possible reasons for this may be firstly that the hollow alloy model corresponds to the global potential energy minimum or secondly that there is insufficient kinetic energy in the system to adequately sample configuration space implying that the hollow model corresponds to a local potential energy minimum. In order to decide which of these possibilities is most probable a second MD simulation was run. The results of this run are given below as the Erkoς c(4 × 4) result 2.

- **Erkoς c(4 × 4) Result 2**

The initial temperature of this MD run was set to 300K. This initial temperature should provide adequate sampling of configuration space. The initial configuration was set to that of the hollow alloy model. On completion of the MD run, figure 4.23 below resulted. The final crystal temperature was 310K. From figure 4.23 it

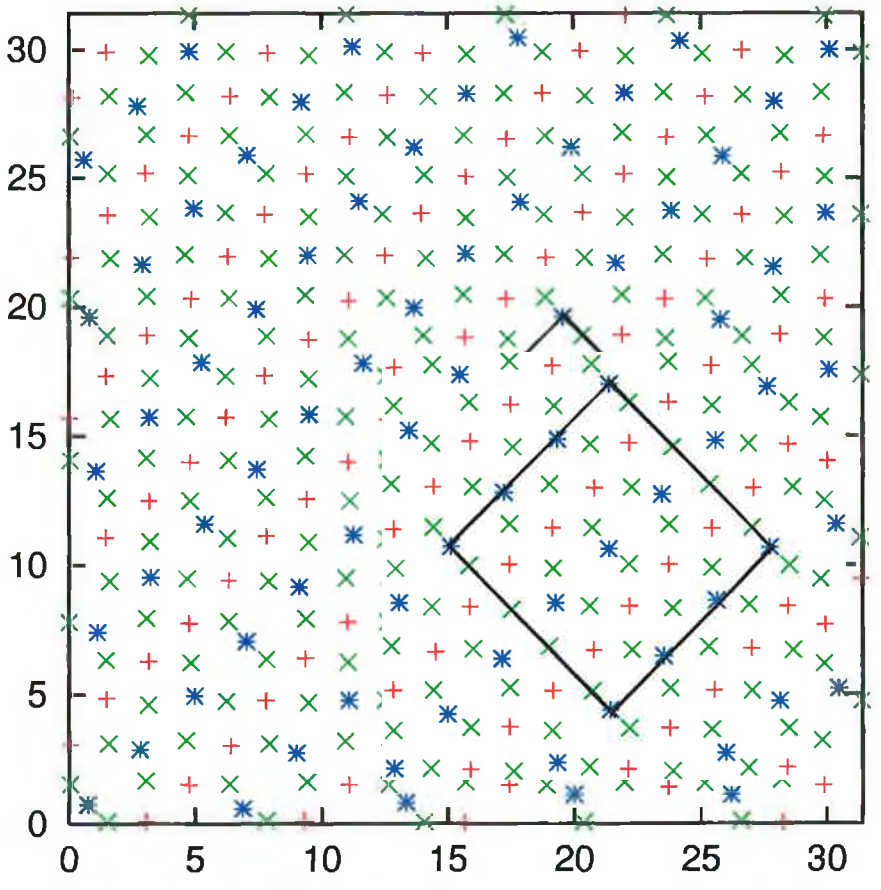

Figure 4.23: Erkoc result2 - c(4 × 4) reconstruction. Atoms marked green designate the uppermost copper substrate layer. Atoms marked red and blue represent the alloy copper and alloy lead respectively.

is clear that the lead-copper alloy coordinates have shifted to new positions that correspond with the bridge alloy model as shown in figure 3.11 [4]. The fact that an initial temperature of 300K gave a different result to that of the MD simulation with an initial temperature of 0K(final temperature of 30K) indicates that at T=30K there was insufficient kinetic energy to adequately sample configuration space. It

can be concluded that the MD simulation of the c(4 × 4) reconstruction, using the three-body Erkoς potential, favours the bridge alloy model. This agrees with the Lennnard-Jones MD simulation of the c(4 × 4) structure in the current study. It also agrees with the STM study of Nagl et al.[3]. It is in disagreement with with the I/V LEED calculation of Gauthier et al [4], in which the hollow alloy model is favoured. One of the differences between the Lennard-Jones c(4 × 4) result and the Erkoς c(4 × 4) result is demonstrated by figure 4.24 below. This is a depth profile of the c(4 × 4) system when modeled using the Erkoς potential. The alloy lead layer is labeled Pb-A in figure 4.24 below. The Erkoς alloy lead in figure 4.23 exhibits no modulation in the z direction as was found for the similar Lennard-Jones result. The lead atoms at bridge sites in figure 4.23 are not raised as occured with the Lennard-Jones result in figure 4.20. This is evidenced in figure 4.24 by the fact that the alloy lead layer(Pb-A) is not split into two sub-peaks as occured for the Lennard-Jones result in figure 4.21 in which an alloy lead z modulation was present. Also it was noted that the substrate peaks Cu1 and Cu2 have each split into two sub-peaks. This did not occur for the Lennard-Jones result as shown in figure 4.21.

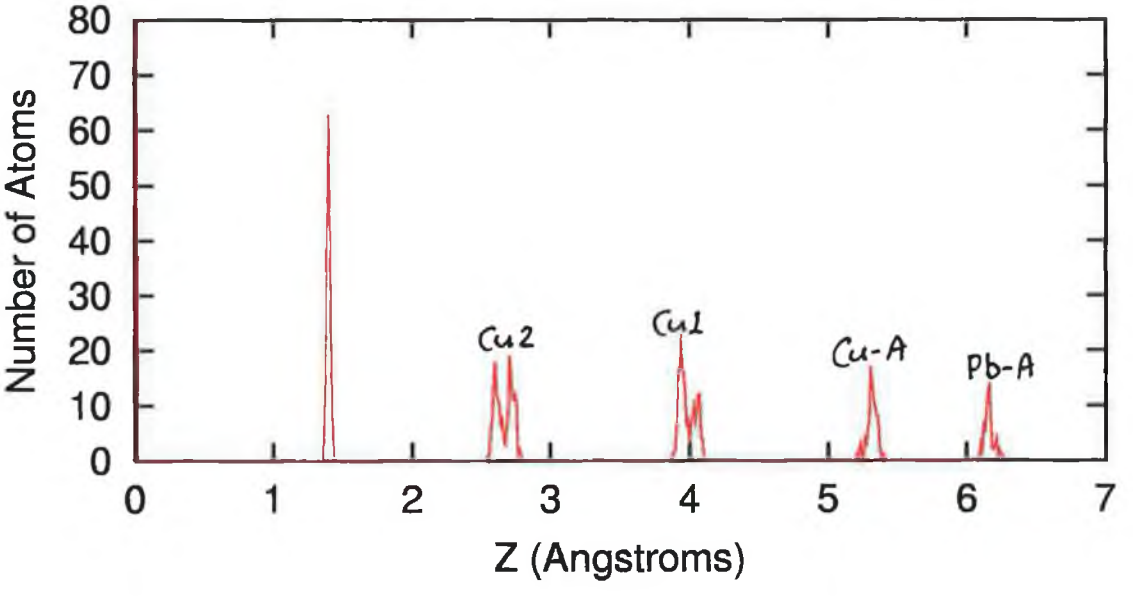

Figure 4.24: Erkoς result2 - c(4 × 4) z distribution. The alloy copper and alloy lead are labeled Cu-A and Pb-A respectively. The uppermost copper substrate layer is labeled Cu1. The next copper substrate layer is labeled Cu2.

4.1.3 Alloy copper lateral modulation

It was noted in a Monte Carlo simulation [6] of the c(4 × 4) reconstruction that a modulation of the alloy copper occured. A similar result was obtained in the I/V LEED calculation of Gauthier et al as shown in figure 3.12. The period of this modulation was stated to be approximately 8 copper-copper distances. Also adjacent chains of the alloy copper were stated to be 180° out of phase.

In the current study a modulation of the alloy copper occured for both the Lennard-Jones and Erkoς simulations. The Lennard-Jones alloy copper coordinates were extracted from the data used to plot the alloy copper in figure 4.20, the alloy copper being those atoms marked by red crosses. Similarly the Erkoς alloy copper coordinates were extracted from the data used to plot the alloy copper in figure 4.23.

A figure of the Lennard-Jones alloy copper is given below in figure 4.25. The four

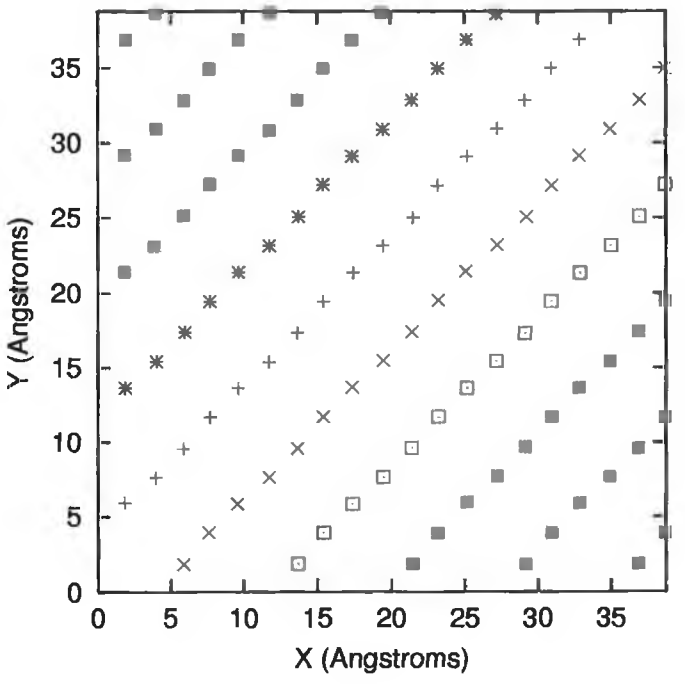

Figure 4.25: LJ c(4x4) alloy copper chains shown here

longest chains are coloured blue, red, green and cyan. In order to view the modulation more clearly each of the four chains has been laterally rotated in a clockwise

direction through 45° about ideal copper lattice points in such a way that the relative intra-chain positions are maintained. After rotating the chains each chain was shifted by an arbitrary amount in the y direction so that the chains could be compared clearly. The peak to peak value of the amplitude remains unaffected by the rotation. The result of this rotation is given below in figure 4.26. Again the chains are coloured identically to the those in figure 4.25, maintaining the correspondence between diagrams. From figure 4.26 it can be seen that there is a very clear lateral

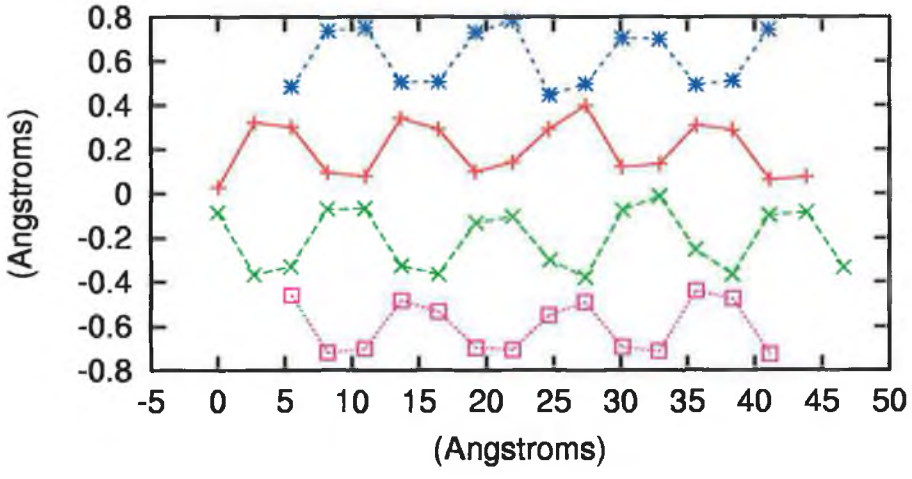

Figure 4.26: LJ c(4x4) highlighted chains rotated

modulation of the alloy copper chains. Adjacent chains are seen to be 180° out of phase while every second chain is in phase. The amplitude of the modulation is approximately 0.37 ± 0.024Å. The period of the modulation is 4 copper-copper distances. The Erkoς result was considered in an identical manner. The alloy copper layer is shown below in figure 4.27. These four chains were rotated in an identical manner to the Lennard-Jones result. The rotated chains are given below in figure 4.28. It is found that adjacent chains are again 180° out of phase. The period of the modulation is 4 copper-copper distances and the approximate amplitude of the modulation is 0.31 ± 0.04Å.

From the results of the alloy copper modulations it can be concluded that a lateral modulation occurs on the alloy copper chains. The amplitude of the modulation was found to be approximately $0.3\mathring{A}$. The period of the modulation is 4

copper-copper distances with adjacent chains being 180° out of phase. This result is in agreement with the result obtained by Tan et al [6], however Tan's result gave a value of 8 copper-copper distances for the period of the modulation.

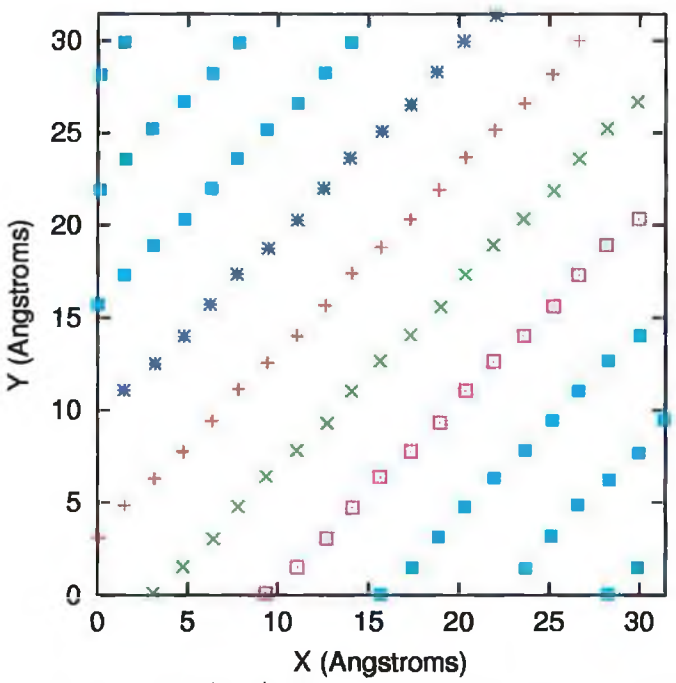

Figure 4.27: LJ c(4x4) alloy copper chains shown here

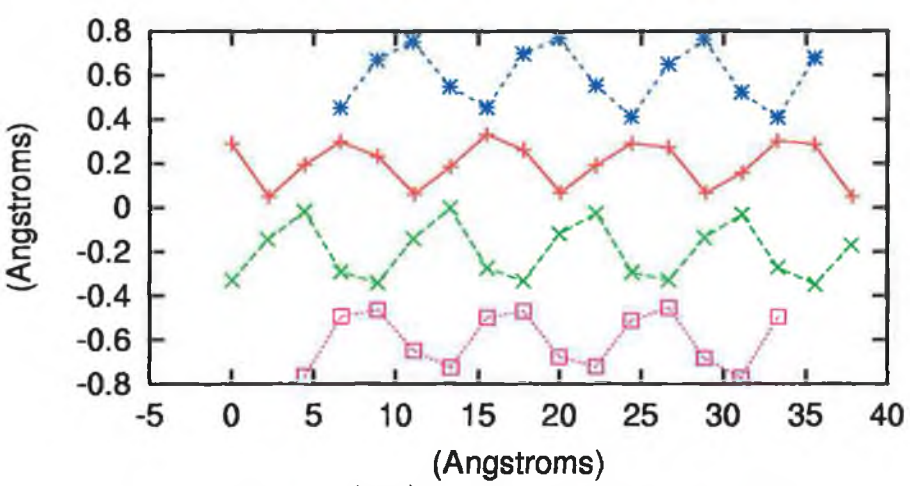

Figure 4.28: LJ c(4x4) highlighted chains rotated

4.2 The c(2 × 2) reconstruction

The details of the c(2 × 2) are well established with the c(2 × 2) reconstruction being a common structure when certain metals are deposited on the (100) face of copper [11], [12].

The initial configuration for the c(2 × 2) reconstruction in the current MD simulation was set to that of the c(2 × 2) structure. The 'bestZs' program discussed in section 2.5.3 was used to obtain crystal z coordinates that would limit the temperature below the melting point of the c(2 × 2) reconstruction. The initial temperature was set to 300K. Two MD runs were completed. The first run used the Lennard-Jones potential, the second used the Erkoς potential.

The results of the MD runs are given in figures 4.29 and 4.30 below. The uppermost copper substrate layer is marked green with the overlayer lead marked red. As can be seen from the diagrams the c(2 × 2) structure remains. There was no extra structure of interest detected from the analysis of both results.

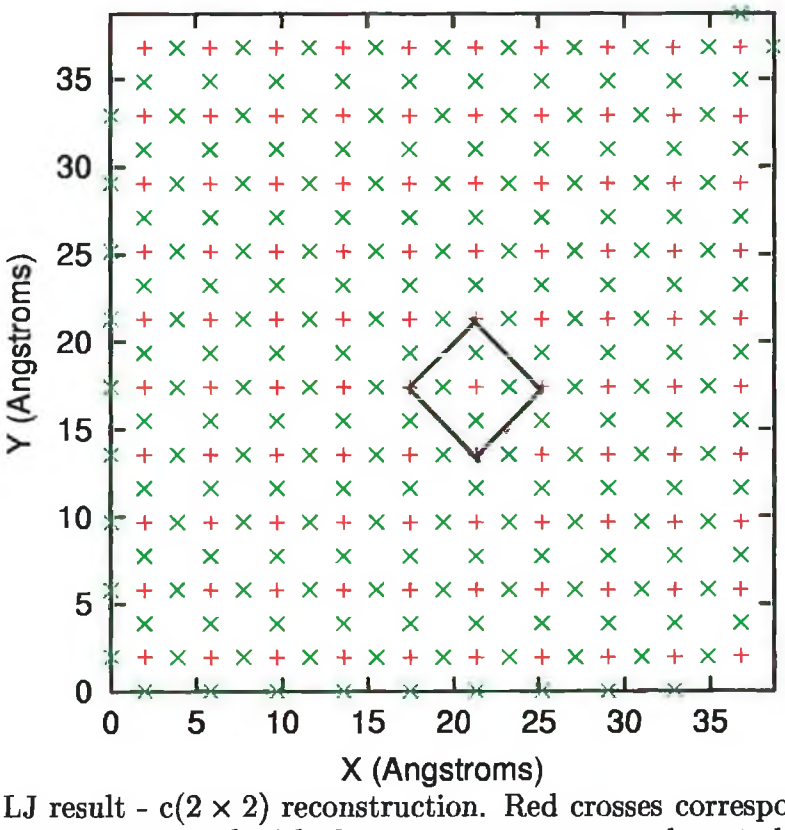

Figure 4.29: LJ result - c(2 × 2) reconstruction. Red crosses correspond with lead while green crosses correspond with the uppermost copper substrate layer

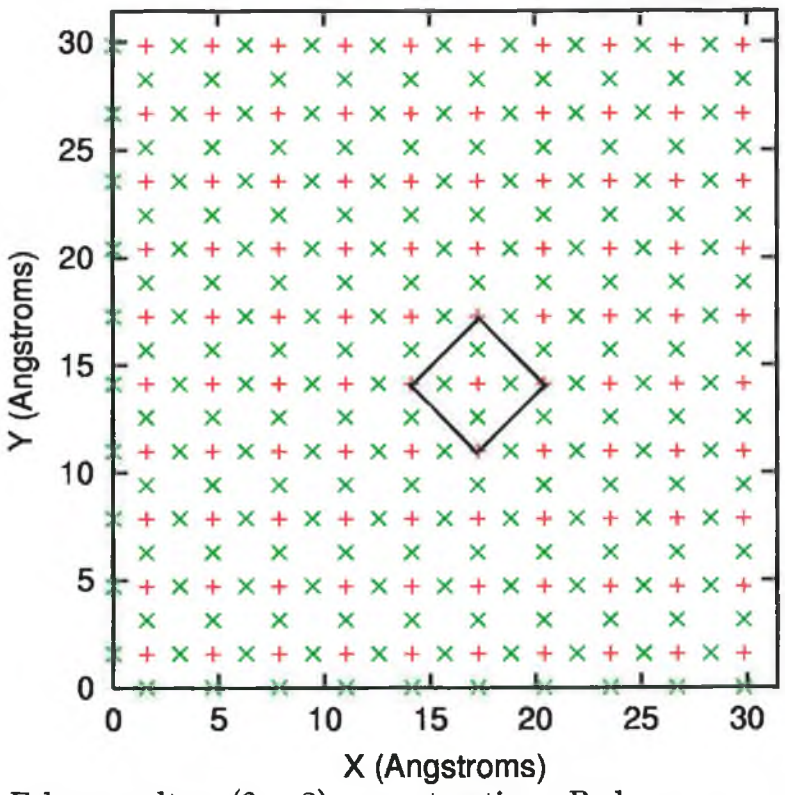

Figure 4.30: Erkoς result - c(2 × 2) reconstruction. Red crosses correspond with lead while green crosses correspond with the uppermost copper substrate layer

A hard sphere 3D representation of the Lennard-Jones result is given below in figures 4.29a, 4.29b and 4.29c.

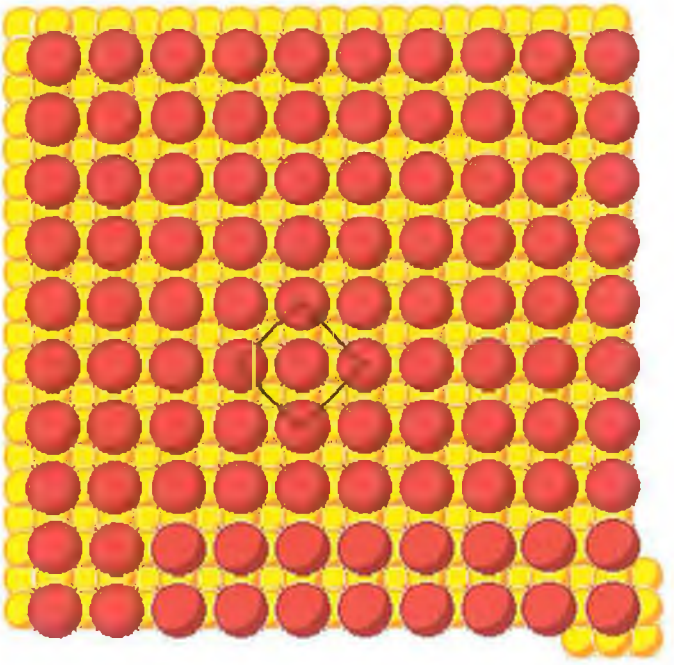

Figure 4.29a : c(2x2) reconstruction, face-on view. Unit cell shown

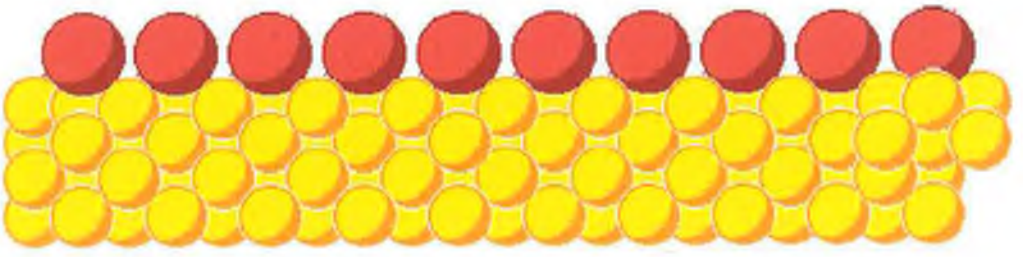

Figure 4.29b : c(2x2) reconstruction, side view

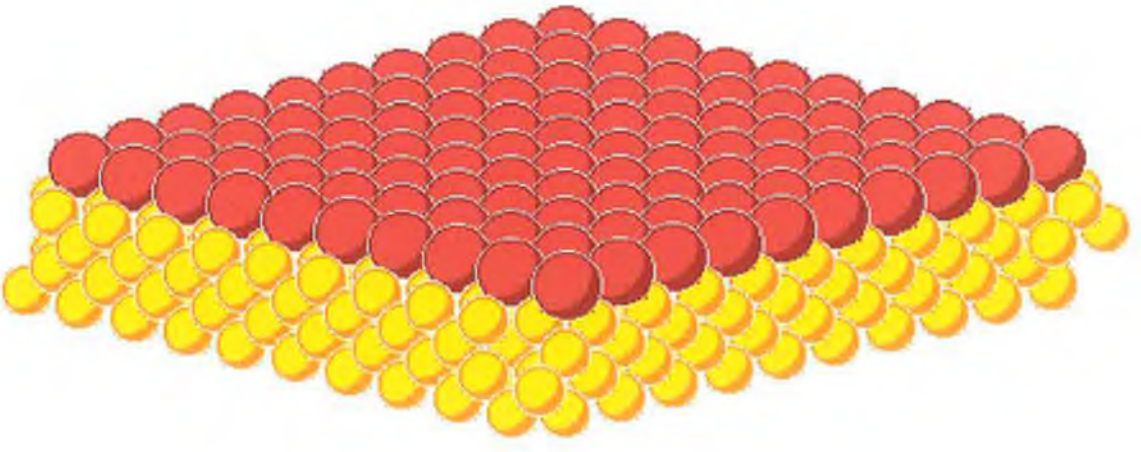

Figure 4.29c : c(2x2) reconstruction, edge-on view

4.3 The c($5\sqrt{2} \times \sqrt{2}$)R45° structure

This section contains the results of the MD simulation of the c($5\sqrt{2} \times \sqrt{2}$)R45° structure when modeled using both the two-body Lennard-Jones [6] and three-body Erkoς [7] potentials. The initial lead positions for every MD run of the c($5\sqrt{2} \times \sqrt{2}$)R45° structure was set to that of Henrion and Rhead [1] as shown in figure 3.14. It was hoped that as the MD system evolved in MD time, the positions of the lead atoms would reorganise to the positions of the accepted(true) reconstruction for the c($5\sqrt{2} \times \sqrt{2}$)R45° structure, as shown in figures 3.15 and 3.16. The results for the Lennard-Jones and Erkoς potentials are given in the following two sections.

4.3.1 Lennard-Jones c($5\sqrt{2} \times \sqrt{2}$)R45° MD results

In a similar study [6] to the current one, the Lennard-Jones potential, described in section 3.5.1, was used in a Monte-Carlo (MC) simulation of the deposition of lead on the (100) face of copper. Starting with the initial configuration of Henrion and Rhead (HR)[1], as in figure 3.14, a MC relaxation was carried out. It was found that, starting with the HR configuration the system aquired a minimum potential energy configuration identical to the accepted model for the c($5\sqrt{2}\times\sqrt{2}$)R45° reconstruction (figures 3.15 and 3.16). This is the motivation for using the HR model as the starting positions for the lead overlayer. There are two separate MD results presented for the Lennard-Jones potential. Either the initial conditions or the cooling of the crystal differ between these two results.

- **Lennard-Jones c($5\sqrt{2} \times \sqrt{2}$)R45° Result 1**

The first Lennard-Jones c($5\sqrt{2}\times\sqrt{2}$)R45° MD run was carried out by depositing the lead atoms one at a time as the MD simulation began. This was an initial effort at reducing the strain heating. By depositing the lead atoms one at a time and letting each atom find its equilibrium position it was hoped that the crystal temperature would remain below the melting point (495K) of the c($5\sqrt{2} \times \sqrt{2}$)R45° structure. The exact coordinates of the lead atoms corresponded with those of the HR [1] model as shown in figure 3.14. The z positions of the atoms, or height above the

substrate surface, was chosen approximately and not subject to any stra[illegible]uction conditions as discussed in section 2.5.3. By using these set of initial [illegible]ions it was found that the temperature of the system increased rapidly beyond the melting point. The lead coordinates were seen to randomize which indicated a melting of the overlayer. To avoid this the system was cooled once the overlayer was deposited. By taking out some of the kinetic energy as the system evolved the melting of the lead overlayer was avoided. When the MD run was completed the overlayer structure below was seen to form. From figure 4.31 it can be seen that up to

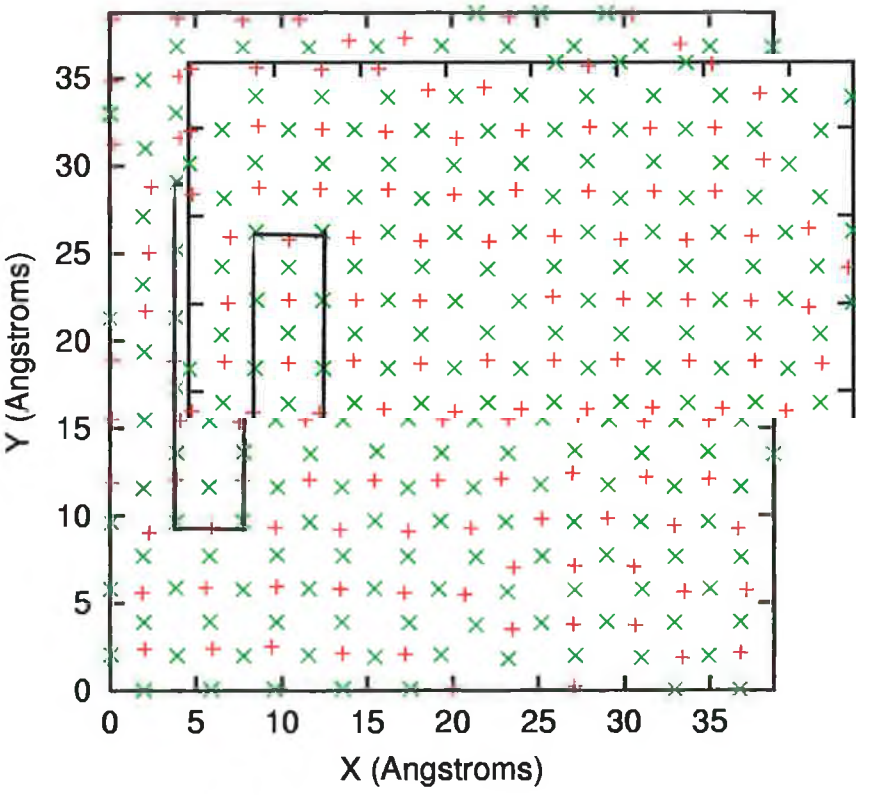

Figure 4.31: result1 - c($5\sqrt{2} \times \sqrt{2}$)R45° reconstruction. Atoms marked green correspond with the uppermost copper substrate layer and the lead overlayer is marked red.

70% of the overlayer structure corresponds with the accepted structure shown in figures 3.15 and 3.16. A hard sphere 3D representation of figure 4.31 is given in figures 4.31a, 4.31b and 4.31c below. As mentioned in section 3.4 the c($5\sqrt{2} \times \sqrt{2}$) structure consists of regions of three rows of c(2×2) separated by anti-phase domain

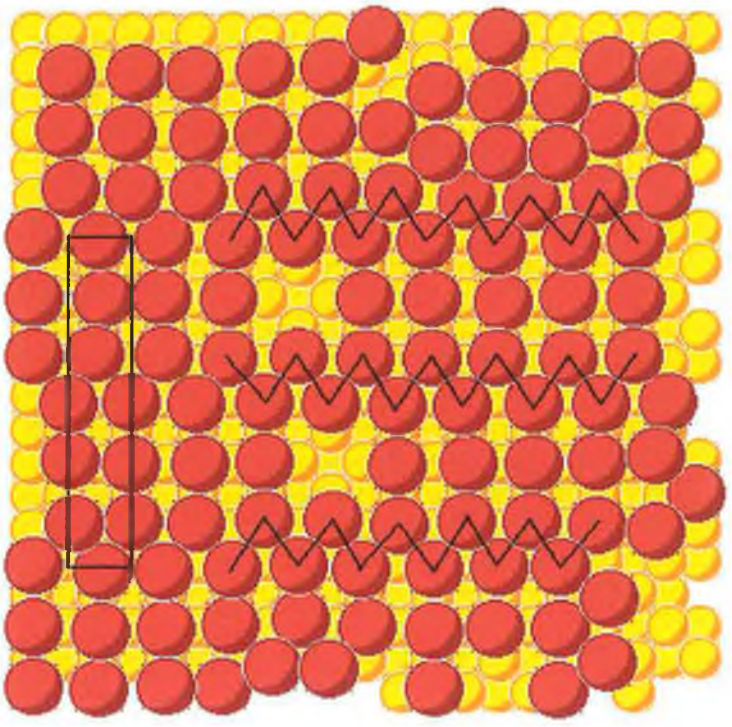

Figure 4.31a : c(5$\sqrt{2}$x$\sqrt{2}$)R 45° reconstruction, face-on view. Unit cell and anti-phase domain boundaries are shown

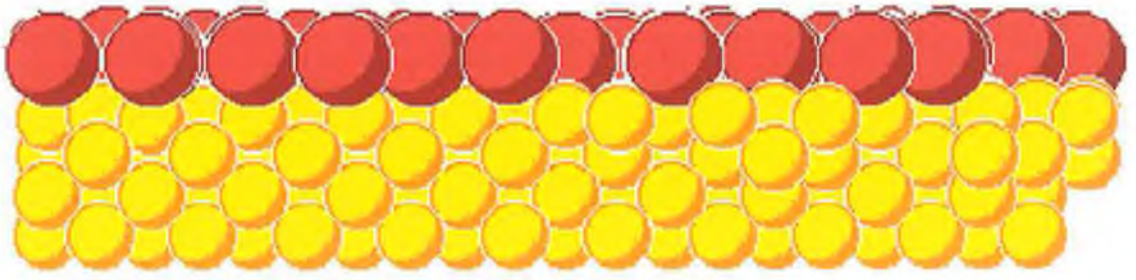

Figure 4.31b : c(5$\sqrt{2}$x$\sqrt{2}$)R 45° reconstruction, side view

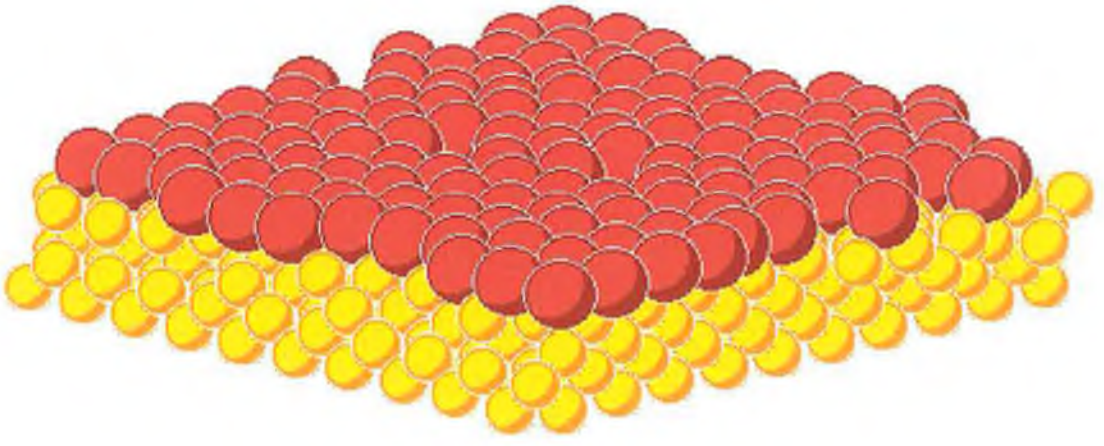

Figure 4.31c : c(5$\sqrt{2}$x$\sqrt{2}$)R 45° reconstruction, edge-on view

boundaries as marked in figure 4.31a. This is the accepted model for the c($5\sqrt{2}\times\sqrt{2}$) reconstruction.

- **Lennard-Jones c($5\sqrt{2} \times \sqrt{2}$)R45° Result 2**

The second Lennard-Jones c($5\sqrt{2} \times \sqrt{2}$)R45° MD run was carried out by depositing the entire lead overlayer on the copper substrate before the run was started. It was found, using this initial condition and an approximate z coordinate for the overlayer, that the crystal temperature rose to a value well above the melting point (495K) of the c($5\sqrt{2} \times \sqrt{2}$)R45° superstructure. The abrupt temperature rise was caused by the fact that the overlayer had an approximate initial z value which resulted in excess strain being introduced into the system as described in section 2.5.3. When the MD run was started, this strain was translated into kinetic energy resulting in the melting of the overlayer. To reduce the initial strain, a new z coordinate was found using the strain reduction program described in section 2.5.3. Starting with the new (reduced-strain overlayer) z coordinate the MD program was started. The system came to equilibrium at 300K which is well below the overlayer melting point of 495K, as required. When the MD run was completed the structure in figure 4.32 below was seen to form. From the figure it is found that approximately 40% of the

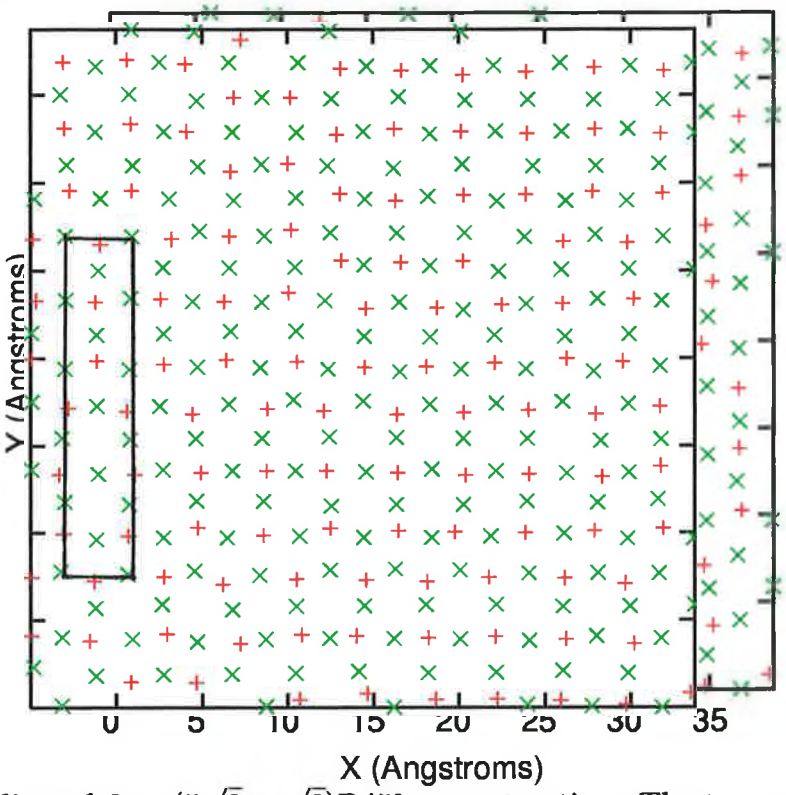

Figure 4.32: lj result2 - c($5\sqrt{2} \times \sqrt{2}$)R45° reconstruction. The top substrate layer is marked green with the lead overlayer marked red.

overlayer structure corresponds with the accepted structure for the $c(5\sqrt{2}\times\sqrt{2})R45°$ reconstruction as shown in figures 3.15 and 3.16.

4.3.2 Erkoς $c(5\sqrt{2} \times \sqrt{2})R45°$ MD results

The three-body Erkoς [7] potential was also used to study the $c(5\sqrt{2} \times \sqrt{2})R45°$ structure. The initial lead configuration was identical to that of the model of Henrion and Rhead [1], as shown in figure 3.14. Initially, as occured with the Lennard-Jones MD runs, the temperature rose abruptly to a temperature well above the melting point of the lead overlayer when an approximate overlayer z value was chosen. The strain-reduction program was used to find an overlayer z value which would limit the strain-heating to a temperature below the melting point (495K) of the overlayer. When the MD run was complete the overlayer configuration in figure 4.33 below resulted. This structure is identical to the initial Henrion and

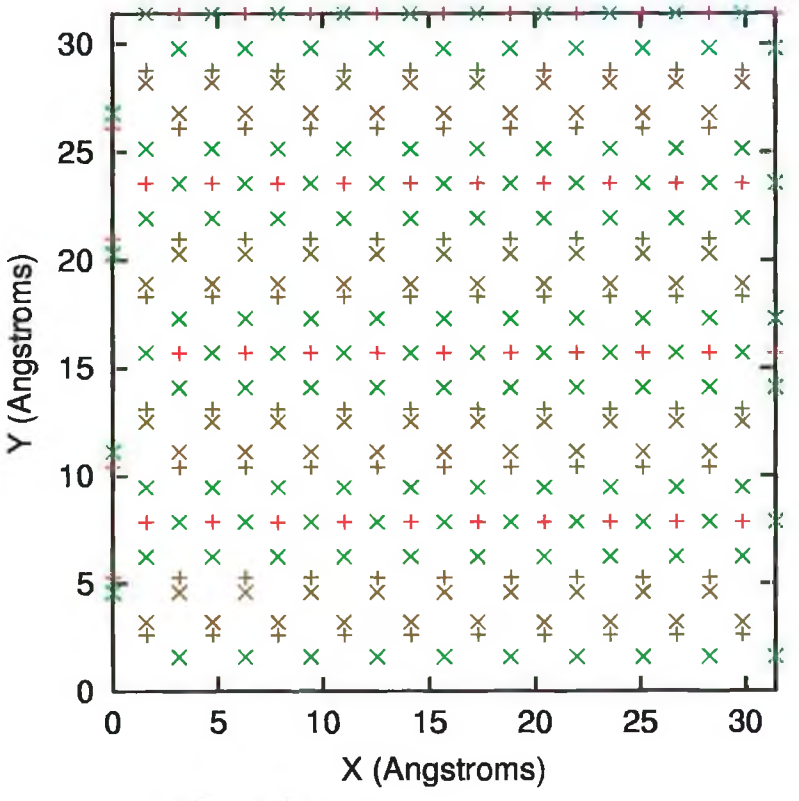

Figure 4.33: Erkoς - $c(5\sqrt{2} \times \sqrt{2})R45°$ reconstruction. The uppermost substrate layer is marked green and the lead overlayer is marked red.

Rhead structure (figure 3.14) which indicates that possibly the strain-reduction program gave a resulting initial configuration, the global potential energy of which, was confined to a local minimum potential energy.

4.4 Conclusions

Using the Molecular Dynamics technique the three reconstructions that form when lead is deposited on the (100) face of copper were studied. The three reconstructions were the c(4×4) , c(2×2) and the c$(5\sqrt{2} \times \sqrt{2})$R45° structures.

The details of the c(4×4) reconstruction are not well understood. It has been ascertained that the most probable structures are the hollow alloy model or the bridge alloy model. Both of these models are single layer alloy models which is unusual for a metal-metal interface. Using the MD technique the aim was to ascertain which of these two models was the most probable. Using an initial configuration corresponding to the hollow alloy model the MD simulation was run. The results for both the two-body Lennard-Jones potential and the three-body Erkoς potential both pointed to the conclusion that the bridge alloy model was the most probable configuration for the c(4×4) reconstruction using the MD technique. This was in agreement with an STM study **[3]** which also concluded that the bridge alloy model was the most probable model for the c(4×4) reconstruction. However it is in disagreement with an I/V LEED calculation **[4]** which concludes that the hollow alloy model is the most probable structure for the c(4×4) reconstruction. It should be noted that the LEED study did not allow the lead chains freedom to move in the z direction. In the current MD study a z modulation was found for the Lennard-Jones potential where the lead atoms situated on bridge sites were slightly raised. This was also noted in the STM study **[3]**. The current MD result for the c(4×4) reconstruction using the Erkoς potential did not show any sign of a modulation of the lead chains in the z direction. A lateral modulation was also noted in the alloyed copper atoms. The amplitude of the modulation was 0.37 ± 0.024Å for the Lennard-Jones potential and 0.31 ± 0.04Å for the Erkoς potential. The period of this modulation is 4 copper-copper distances. A lateral modulation was also noticed in the studies of Tan **[6]** and Gauthier **[4]**. The amplitude of the modulation is not given in both cases. The period of the modulation in the case of Tan's study was stated to be 8

copper-copper distances.

The c(2 × 2) structure is a relatively simple structure whose details are well understood, however it was included for completeness. On completion of the c(2 × 2) MD run there were no modulations of the lead overlayer or the uppermost substrate layer. The initial configuration was that of the exact c(2 × 2) model. When the simulation finished the c(2 × 2) structure remained.

The details of the c($5\sqrt{2} \times \sqrt{2}$)R45° structure are well established. This reconstruction consists of bands of three rows of the c(2 × 2) structure separated by anti-phase domain boundaries as shown in figure 4.31a. The initial configuration for this reconstruction was the hexagonal structure of Henrion and Rhead [1]. On completion of the MD run the structure in figure 4.31a resulted. As can be seen from the diagram the anti-phas domain boundaries are very clear. Also there are three rows of c(2 × 2) structure between boundaries. Thus the accepted structure for the c($5\sqrt{2} \times \sqrt{2}$)R45° reconstruction has been evolved from an initial hexagonal type structure.

Any future work could be directed towards the simulation of the deposition of various metals on the (100) face of copper, such as Sn on copper. A list of the Erkoς potential parameters for various metals can be found in the paper of Erkoς [7].

Chapter 5 References

[1] : J. Henrion and G. E. Rhead - Surf. Sci. 29(1972)20-36

[2] : A. Sepulveda and G. E. Rhead - Surf. Sci. 66(1977)436-448

[3] : C. Nagl, E. Platzgummer, O. Haller, M. Schmid, P. Varga - Surf. Sci. 331-333(1995)831-837

[4] : Y. Gauthier, W. Moritz, W. Hosler - Surf. Sci. 345(1996)53-63

[5] : S. Robert, S. Gauthier, F. Bocquet, S. Rousset, J.L. Duvault, J. Klein - Surf. Sci. 350(1996)136-144

[6] : S. Tan, A. Ghazali, J.C.S. Levy - Surf. Sci. 377-379(1997)15-17

[7] : Sakir Erkoc - Physics Reports 278(1997)79-105 - Section 2.2.14

[8] : M. Dreschler in : Basic Problems in Thin Film Physics. Eds. R. Niedermayer and H. Mayen (Vandenhoeck and Ruprecht, Gottingen, 1996)p18

[9] : C. Nagl, O. Haller, E. Platzgummer, M. Schmid, P. Varga - Surf. Sci. 321(1994)237-

[10] : D.C. Rapaport : The Art of Molecular Dynamics Simulation, Cambridge (1995)

[11] : S. Mizuno, H. Tochiara, T. Kawamura - Surf. Sci. 293(1993)239-

[12] : A. Mikkelsen, D.L. Adams - Phys. Rev. B 60(1999)2040

[13] : Van Hove M. (1995), Software packages SARCH/LATUSE/PLOT3D Version 4.01, http://electron.lbl.gov/webmain.html

Chapter 6 Appendices

6.1 Appendix A

The *Erkoς* potential energy function (PEF)is given here. It is then differentiated with respect to position ie. x, y or z. The full derivation of thid differentiation is given below.

The *Erkoς* PEF is given by,

$$V_{i,jk} = U_{ij} + U_{ik} + C_3 U_{ij} f_{ijk} + C_3 U_{ik} f_{ikj} + C_3 U_{jk} f_{jki} \tag{24}$$

where

$$U_{ij} = C_2 A \left\{ \frac{r_0^{2n}}{r_{ij}^{2n}} \exp(-2\alpha \frac{r_{ij}^2}{r_0^2}) \; - \; \frac{r_0^n}{r_{ij}^n} \exp(-\alpha \frac{r_{ij}^2}{r_0^2}) \right\}$$

and

$$f_{ijk} = \exp(-\frac{r_{ik}^2 + r_{jk}^2}{r_0^2})$$

The objective of the differentiation is to obtain an expression for the force on particle i due to particles j and k. The force on i due to the j, k pair is labeled $\mathbf{f}_{i,jk}^{\gamma}$, where γ represents the directions x,y or z. The force expression is equal to the negative of the gradient of the PEF, ie.

$$\mathbf{f} = -\nabla V$$

$$\vec{\mathbf{f}} = -\frac{\partial V_{i,jk}}{\partial x_i}\vec{\mathbf{i}} - \frac{\partial V_{i,jk}}{\partial y_i}\vec{\mathbf{j}} - \frac{\partial V_{i,jk}}{\partial z_i}\vec{\mathbf{k}}$$

where

$\vec{\mathbf{f}}$	= vector force
V	= Potential energy function
∇V	= gradient of PEF
x_i, y_i, z_i	= component variables of particle i
$\vec{\mathbf{i}}, \vec{\mathbf{j}}, \vec{\mathbf{k}}$	= unit vectors

The PEF $V_{i,jk}$ needs to be differentiated with respect to x_i, y_i and z_i. If r_i^γ is to represent x_i, y_i and z_i then the required differential is $\partial V_{i,jk}/r_i^\gamma$. By differentiating equation (24) term by term we get,

$$\frac{\partial V_{i,jk}}{\partial r_i^\gamma} = \frac{\partial U_{ij}}{\partial r_i^\gamma} + \frac{\partial U_{ik}}{\partial r_i^\gamma} + C_3\frac{\partial U_{ij} f_{ijk}}{\partial r_i^\gamma} + C_3\frac{\partial U_{ik} f_{ikj}}{\partial r_i^\gamma} + C_3\frac{\partial U_{jk} f_{jki}}{\partial r_i^\gamma} \tag{25}$$

There are five terms in this expression. Each term shall be considered individually. Term one is,

$$\frac{\partial U_{ij}}{\partial r_i^\gamma}$$

$$U_{ij} = \underbrace{C_2 A r_0^{2n} r_{ij}^{-2n} \exp(-2\alpha\frac{r_{ij}^2}{r_0^2})}_{\text{P}} \; - \; \underbrace{C_2 A r_0^{n} r_{ij}^{-n} \exp(-2\alpha\frac{r_{ij}^2}{r_0^2})}_{\text{Q}}$$

$$\frac{\partial U_{ij}}{\partial r_i^\gamma} = \frac{\partial P}{\partial r_i^\gamma} \; - \; \frac{\partial Q}{\partial r_i^\gamma} \tag{26}$$

If we let $C_2 A r_0^{2n} = S$ and $2\alpha/r_0^2 = T$ then P becomes,

$$P = S r_{ij}^{-2n} \exp(-T r_{ij}^2)$$

then

$$\frac{\partial P}{\partial r_i^\gamma} = S\left\{ r_{ij}^{-2n} \exp()(-T\frac{\partial r_{ij}^2}{\partial r_i^\gamma}) \; + \; \exp()(-2n r_{ij}^{-2n-1})\frac{\partial r_{ij}}{\partial r_i^\gamma} \right\} \tag{27}$$

where

$$\exp() = \exp(-T r_{ij}^2)$$

From equation (18)

$$\frac{\partial r_{ij}}{\partial r_i^\gamma} = \frac{\Delta r_{ij}^\gamma}{r_{ij}}$$

but

$$\frac{\partial r_{ij}^2}{\partial r_i^\gamma} = 2 r_{ij}\frac{\partial r_{ij}}{\partial r_i^\gamma}$$

so

$$\frac{\partial r_{ij}^2}{\partial r_i^\gamma} = 2\Delta r_{ij}^\gamma \tag{28}$$

Using equations (18) and (28) expression (27) becomes,

$$\frac{\partial P}{\partial r_i^\gamma} = S\left\{2r_{ij}^{-2n}\Delta r_{ij}^\gamma \exp(-Tr_{ij}^2)(-T - nr_{ij}^{-2})\right\}$$

so putting back in for S and T we get,

$$\frac{\partial P}{\partial r_i^\gamma} = 2C_2A\Delta r_{ij}^\gamma r_0^n r_{ij}^{-n}\exp(-\alpha\frac{r_{ij}^2}{r_0^2})\left\{-\frac{2\alpha}{r_0^2} - \frac{n}{r_{ij}^2}\right\}$$

Now by letting

$$\omega_{ij} = \frac{2\alpha}{r_0^2} + \frac{n}{r_{ij}^2}$$

and

$$\tau_{ij} \;=\; r_0^n r_{ij}^{-n}\exp(-\alpha\frac{r_{ij}^2}{r_0^2})$$

we get,

$$\frac{\partial P}{\partial r_i^\gamma} = -2C_2A\Delta r_{ij}^\gamma \omega_{ij}\tau_{ij}^2 \tag{29}$$

Similarly,

$$\frac{\partial Q}{\partial r_i^\gamma} = -C_2A\Delta r_{ij}^\gamma \omega_{ij}\tau_{ij} \tag{30}$$

Substituting (29) and (30) into (26) we have term 1 in equation (25),

$$\frac{\partial U_{ij}}{\partial r_i^\gamma} = -C_2A\Delta r_{ij}^\gamma \omega_{ij}\tau_{ij}(2\tau_{ij} - 1) \tag{31}$$

Similarly term 2 becomes,

$$\frac{\partial U_{ik}}{\partial r_i^\gamma} = -C_2A\Delta r_{ik}^\gamma \omega_{ik}\tau_{ij}(2\tau_{ik} - 1) \tag{32}$$

We now need to evaluate term 3 of equation (25) ie.

$$C_3\frac{\partial U_{ij}f_{ijk}}{\partial r_i^\gamma}$$

Differentiating we get,

$$C_3\frac{\partial U_{ij}f_{ijk}}{\partial r_i^\gamma} = C_3\left\{U_{ij}\frac{\partial f_{ijk}}{\partial r_i^\gamma} \;+\; f_{ijk}\frac{\partial U_{ij}}{\partial r_i^\gamma}\right\} \tag{33}$$

We now need to find $\partial f_{ijk}/\partial r_i^\gamma$

$$f_{ijk} = \exp(\frac{-r_{ik}^2 - r_{jk}^2}{r_0^2})$$

$$\frac{\partial f_{ijk}}{\partial r_i^\gamma} = -r_0^{-2} \exp\left(\frac{-r_{ik}^2 - r_{jk}^2}{r_0^2}\right) \left\{ \frac{\partial r_{ik}^2}{\partial r_i^\gamma} + \frac{\partial r_{jk}^2}{\partial r_i^\gamma} \right\} \tag{34}$$

but

$$\frac{\partial r_{ik}^2}{\partial r_i^\gamma} = 2\Delta r_{ik}^\gamma$$

and

$$\frac{\partial r_{jk}^2}{\partial r_i^\gamma} = 2r_{jk} \frac{\partial r_{jk}}{\partial r_i^\gamma}$$

and

$$\frac{\partial r_{jk}}{\partial r_i^\gamma} = 0$$

therefore equation (34) becomes,

$$\frac{\partial f_{ijk}}{\partial r_i^\gamma} = \frac{-2\Delta r_{ik}^\gamma}{r_0^2} f_{ijk} \tag{35}$$

Substituting equations (31) and (35) into equation (33) we get,

$$C_3 \frac{\partial U_{ij} f_{ijk}}{\partial r_i^\gamma} = -C_3 C_2 A f_{ijk} \tau_{ij} \left\{ \frac{2\Delta r_{ik}^\gamma}{r_0^2} (\tau_{ij} - 1) + \Delta r_{ij}^\gamma \omega_{ij} (2\tau_{ij} - 1) \right\} \tag{36}$$

Equation (36) represents term 3 of equation (25). Term 4 is similarly obtained ie.

$$C_3 \frac{\partial U_{ik} f_{ikj}}{\partial r_i^\gamma} = -C_3 C_2 A f_{ikj} \tau_{ik} \left\{ \frac{2\Delta r_{ij}^\gamma}{r_0^2} (\tau_{ik} - 1) + \Delta r_{ik}^\gamma \omega_{ik} (2\tau_{ik} - 1) \right\} \tag{37}$$

The final term of equation (25) is,

$$C_3 \frac{\partial U_{jk} f_{jki}}{\partial r_i^\gamma}$$

Differentiating we get,

$$C_3 \frac{\partial U_{jk} f_{jki}}{\partial r_i^\gamma} = C_3 \left\{ U_{jk} \frac{\partial f_{jki}}{\partial r_i^\gamma} + f_{jki} \frac{\partial U_{jk}}{\partial r_i^\gamma} \right\}$$

but

$$\frac{\partial U_{jk}}{\partial r_i^\gamma} = 0$$

so

$$C_3 \frac{\partial U_{jk} f_{jki}}{\partial r_i^\gamma} = C_3 U_{jk} \frac{\partial f_{jki}}{\partial r_i^\gamma} \tag{38}$$

Now we need $\partial f_{jki}/\partial r_i^\gamma$,

$$f_{jki} = \exp\left(\frac{-r_{ji}^2 - r_{ki}^2}{r_0^2}\right)$$

therefore,

$$\frac{\partial f_{jki}}{\partial r_i^\gamma} = -r_0^{-2}\exp\left(\frac{-r_{ji}^2 - r_{ki}^2}{r_0^2}\right)\left\{\frac{\partial r_{ji}^2}{\partial r_i^\gamma} + \frac{\partial r_{ki}^2}{\partial r_i^\gamma}\right\} \tag{39}$$

but

$$\frac{\partial r_{ji}^2}{\partial r_i^\gamma} = -2\Delta r_{ji}^\gamma = 2\Delta r_{ij}^\gamma$$

and

$$\frac{\partial r_{ki}^2}{\partial r_i^\gamma} = -2\Delta r_{ki}^\gamma = 2\Delta r_{ik}^\gamma$$

thus equation (39) becomes,

$$\frac{\partial f_{jki}}{\partial r_i^\gamma} = -2r_0^{-2} f_{jki}(\Delta r_{ij}^\gamma + \Delta r_{ik}^\gamma) \tag{40}$$

Putting equation (40) into equation (38) we get,

$$C_3\frac{\partial U_{jk} f_{jki}}{\partial r_i^\gamma} = -2C_3C_2A f_{jki}\tau_{jk}r_0^{-2}(\tau_{jk} - 1)(\Delta r_{ij}^\gamma + \Delta r_{ik}^\gamma) \tag{41}$$

This is the final term in equation (25). Substituting all derived terms into equation (25) we get,

$$\begin{aligned}
\frac{\partial V_{i,jk}}{\partial r_i^\gamma} &= -C_2A\Delta r_{ij}^\gamma\omega_{ij}\tau_{ij}(2\tau_{ij} - 1) - C_2A\Delta r_{ik}^\gamma\omega_{ik}\tau_{ik}(2\tau_{ik} - 1) \\
&- C_3C_2A f_{ijk}\tau_{ij}\left\{\frac{2\Delta r_{ik}^\gamma}{r_0^2}(\tau_{ij} - 1) + \Delta r_{ij}^\gamma\omega_{ij}(2\tau_{ij} - 1)\right\} \\
&- C_3C_2A f_{ijk}\tau_{ik}\left\{\frac{2\Delta r_{ij}^\gamma}{r_0^2}(\tau_{ik} - 1) + \Delta r_{ik}^\gamma\omega_{ik}(2\tau_{ik} - 1)\right\} \\
&- 2C_3C_2A f_{jki}\tau_{jk}r_0^{-2}(\tau_{jk} - 1)(\Delta r_{ij}^\gamma + \Delta r_{ik}^\gamma)
\end{aligned} \tag{42}$$

where

$$\begin{aligned}
\Delta r_{ab}^\gamma &= r_a^\gamma - r_b^\gamma \\
\omega_{ab} &= \frac{2\alpha}{r_0^2} + \frac{n}{r_{ab}^2} \\
\tau_{ab} &= r_0^n r_{ab}^{-n}\exp\left(-\alpha\frac{r_{ab}^2}{r_0^2}\right) \\
f_{abc} &= \exp\left(\frac{-r_{ac}^2 - r_{bc}^2}{r_0^2}\right) \\
\alpha &= \log_e(2)
\end{aligned}$$

Finally taking the negative of expression (42) yields the *Erkoς* force expression given in equation (22).